FILE COPY

(2)

NAVAL POSTGRADUATE SCHOOL
Monterey, California

AD-A225 796

DTIC
ELECTE
AUG 27 1990
S D
B
Co

THESIS

DIELECTRIC CHARGING AS A CATALYST TO
THE FORMATION OF POTENTIAL BARRIERS
ON SYNCHRONOUS ORBIT SATELLITES

by

Maude Elizabeth Young

March 1990

Thesis Advisor: Richard C. Olsen

Approved for public release; distribution is unlimited

UNCLASSIFIED

SECURITY CLASSIFICATION OF THIS PAGE

REPORT DOCUMENTATION PAGE

Form Approved OMB No. 0704-0188

1a. REPORT SECURITY CLASSIFICATION UNCLASSIFIED	1b. RESTRICTIVE MARKINGS
2a. SECURITY CLASSIFICATION AUTHORITY	3. DISTRIBUTION/AVAILABILITY OF REPORT Approved for public release; distribution is unlimited
2b. DECLASSIFICATION/DOWNGRADING SCHEDULE	
4. PERFORMING ORGANIZATION REPORT NUMBER(S)	5. MONITORING ORGANIZATION REPORT NUMBER(S)
6a. NAME OF PERFORMING ORGANIZATION Naval Postgraduate School 6b. OFFICE SYMBOL (If applicable) Code 39	7a. NAME OF MONITORING ORGANIZATION Naval Postgraduate School
6c. ADDRESS (City, State, and ZIP Code) Monterey, CA 93943-5000	7b. ADDRESS (City, State, and ZIP Code) Monterey, CA 93943-5000
8a. NAME OF FUNDING/SPONSORING ORGANIZATION 8b. OFFICE SYMBOL (If applicable)	9. PROCUREMENT INSTRUMENT IDENTIFICATION NUMBER
8c. ADDRESS (City, State, and ZIP Code)	10. SOURCE OF FUNDING NUMBERS PROGRAM ELEMENT NO. / PROJECT NO. / TASK NO / WORK UNIT ACCESSION NO.

11. TITLE (Include Security Classification)
DIELECTRIC CHARGING AS A CATALYST TO THE FORMATION OF POTENTIAL BARRIERS ON SYNCHRONOUS ORBIT SATELLITES

12. PERSONAL AUTHOR(S)
Young, Maude E.

13a. TYPE OF REPORT	13b. TIME COVERED	14. DATE OF REPORT (Year, Month, Day)	15. PAGE COUNT
Master's Thesis	FROM _____ TO _____	March 1990	88

16. SUPPLEMENTARY NOTATION The views expressed in this thesis are those of the author and do not reflect the official policy or position of the Department of Defense or the U.S. Government.

17. COSATI CODES			18. SUBJECT TERMS (Continue on reverse if necessary and identify by block number)
FIELD	GROUP	SUB-GROUP	Dielectric, Spacecraft Charging, ISEE1, Potential Barriers

19. ABSTRACT (Continue on reverse if necessary and identify by block number)

This thesis postulates deep dielectric charging of exterior spacecraft dielectrics as a mechanism responsible for the sunlit charging event observed on the ISEE1 spacecraft. Deep dielectric charging can cause a negative potential to develop on the insulating surfaces of spacecraft, resulting in the formation of a potential barrier capable of suppressing photo and secondary emissions. These events can lead to overall negative charging of the spacecraft. Calculations were made using in situ measurements from onboard the ISEE1 and the SCATHA spacecraft. The results indicate, within the range of the data used, that this mechanism is a viable explanation for the ISEE1 charging event. This mechanism can be generalized to most synchronous orbit spacecraft.

20. DISTRIBUTION/AVAILABILITY OF ABSTRACT ☒ UNCLASSIFIED/UNLIMITED ☐ SAME AS RPT. ☐ DTIC USERS	21. ABSTRACT SECURITY CLASSIFICATION UNCLASSIFIED
22a. NAME OF RESPONSIBLE INDIVIDUAL Richard C. Olsen	22b. TELEPHONE (Include Area Code) (408) 646-2019 22c. OFFICE SYMBOL PH/Os

DD Form 1473, JUN 86 Previous editions are obsolete. SECURITY CLASSIFICATION OF THIS PAGE

Approved for public release; distribution is unlimited

Dielectric Charging as a Catalyst to the Formation of Potential Barriers on Synchronous Orbit Satellites

by

Maude E. Young
Lieutenant, United States Navy
B.S., U.S. Naval Academy, 1984

Submitted in partial fulfillment of the requirements for the degree of

MASTER OF SCIENCE IN PHYSICS

from the

NAVAL POSTGRADUATE SCHOOL

March 1990

Author: Maude E. Young
Maude E. Young

Approved by: Richard Chris Olsen
R. C. Olsen, Thesis Advisor

X. K. Maruyama
X. K. Maruyama, Second Reader

K.E. Woehler, Chairman,
Department of Physics

ABSTRACT

This thesis postulates deep dielectric charging of exterior spacecraft dielectrics as a mechanism responsible for the sunlit charging event observed on the ISEE1 spacecraft. Deep dielectric charging can cause a negative potential to develop on the insulating surfaces of the spacecraft, resulting in the formation of a potential barrier capable of suppressing photo and secondary emission. These events can lead to overall negative charging of the spacecraft. Calculations were made using in situ measurements from onboard the ISEE1 and the SCATHA spacecraft. The results indicate, within the range of the data used, that this mechanism is a viable explanation for the ISEE1 charging event. This mechanism can be generalized to most synchronous orbit spacecraft.

DTIC COPY INSPECTED

Accession For
NTIS GRA&I ☒
DTIC TAB ☐
Unannounced ☐
Justification
By
Distribution/
Availability Codes
Dist | Avail and/or Special
A-1

TABLE OF CONTENTS

ACKNOWLEDGMENTS

The author attributes the concept developed in this thesis to A. L. Vampola.

The author wishes to acknowledge the assistance of the following people who provided valuable information and data. P. Mizera, Aerospace Corp., the principle investigator for the SSPM who provided information of the instrument. H. Koons and J. Roeder, Aerospace Corp., produced numerous summary plots of the SSPM data. D. Gorney, and H. Cha, also of the Aerospace Corp., found the precise dates of several satellite upsets and provided them to the author. G. Berzins, R. Belian, and T. Cayton, Los Alamos National Laboratory, provided the SEE and CPA data plots. N. J. Stevens, TRW, obtained the author use of, and provided the DCAT62 code. P. Schemerhorn, Corning Incorp., sent information on various types of Corning glass. A. R. Fredrickson provided his computer code and many valuable discussions, and of course, O. Heinz who was always very encouraging.

I. OVERVIEW

A. DEFINITION AND EFFECTS

1. Spacecraft Charging

Spacecraft charging is the process by which a spacecraft develops a potential relative to the surrounding plasma. The majority of spacecraft charging events have been reported on satellites in geosynchronous orbit. Spacecraft charging at high levels was first reported in 1972 by DeForest [Ref. 1:p. 651-659] on the Applications Technology Satellite (ATS)-5. DeForest associated the high negative potentials recorded on ATS-5 with the injection of hot plasma into synchronous orbit by magnetospheric substorm activity.

Spacecraft charging is important because it has been associated with anomalous satellite behavior, and even system failure. A satellite anomaly is an undesired event in a satellite subsystem such as a spurious detector signal, or an unintended logic reset in an electronic system. This association was first demonstrated by Fredricks and Scarf who noticed in late 1971 several anomalies in the behavior of certain subsystems onboard satellites in synchronous orbit [Ref. 2:p. 277-285]. Out of 23 observed anomalies they correlated 19 definitely, 2 probably, and 2 questionably to ground magnetograms indicating storm or substorm activity in the magnetosphere. Coupled with DeForest's observation of spacecraft charging under the same

circumstances, a strong case was made for a mechanism involving magnetic storm induced spacecraft charging to explain these anomalies. A later study by Pike and Bunn also presents strong statistical evidence correlating anomalies onboard satellites of the Defense Satellite Communications System (DSCS) to magnetospheric substorm activity [Ref. 3:p 45-60]. The anomalies studied were logic reset anomalies, (50 total), converter switching anomalies (9 total), and spinup anomalies (3 total). Ninety percent of the logic reset anomalies, 100% of the converter switching anomalies, and 67% of the spinup anomalies were associated with magnetic substorms. Pike and Bunn, however, pointed out that substorm activity occurs much more frequently than do satellite anomalies. Also ground magnetograms used to infer the state of the magnetosphere are not in situ measurements of the magnetospheric environment. They conservatively concluded that substorm activity may be a factor in producing satellite anomalies and spacecraft charging could be an underlying causative factor. Later work has substantiated these conclusions, and expanded the association between environmental factors and spacecraft anomalies. An entire program, the joint NASA/USAF Spacecraft Charging at High Altitudes (SCATHA) program, was initiated and a satellite (P78-2) was flown in 1979, to study the characteristics of spacecraft charging, and the subsequent satellite response [Ref 4:p 15-30]. SCATHA showed the correlation between spacecraft charging, arcing, and logic upsets (anomalies) [Ref. 5:p. 425-431].

Spacecraft charging is not the only environmental hazard faced by satellites. For instance, other concerns include single event upsets, micrometeorite impacts, and system degradation from accumulated radiation dosage. These perils, however, will not be discussed in this thesis.

2. Types of Spacecraft Charging

There are two types of spacecraft charging, external or surface charging, and the internal charging of dielectrics. Surface charging is the better known phenomenon. It is associated with relatively low energy, 10-80 keV, electrons that traverse geosynchronous orbit as a result of magnetic substorms. Internal charging of dielectrics occurs from the deposition of relatively high energy electrons within the bulk of a dielectric; the electron energy range significant for internal charging is highly material dependent, but ranges from kev to MeV energies.

a. Surface Charging

Surface charging is the most widely studied form of spacecraft charging. It results from the emission and collection of charged particles to and from the surface of the satellite. Since the particles are moving they can be considered as currents, and thus the equilibrium potential of the spacecraft is determined by the balance of these currents and the capacitance of the vehicle. The predominant current sources (in relative order of magnitude) are:

- photoemitted electrons
- ambient electrons
- secondary electrons (true secondary electrons and backscattered electrons).
- ambient ions

Other current sources are secondary electrons from ion impacts, currents generated by the movement of the satellite across local ambient magnetic field lines or relative to the ambient ion populations, and currents from man-made sources such as plasma beams from ion sources. These latter effects are relatively small in magnitude or infrequent in occurrence therefore these sources will not be considered here [Ref. 6:p. 168].

If a spacecraft charges uniformly, as in a completely conducting vehicle, then the absolute potential would only affect a limited number scientific measurements, such as that of plasma fluxes, and poses no operational hazard to the spacecraft. However if part of the spacecraft is electrically isolated from the main spacecraft body, for example a nonconducting thermal blanket, then a charge differential can build up, producing potential gradients that result in large electric fields across the spacecraft. These electric fields pose a serious hazard to the spacecraft by inducing electrical breakdown (arc discharges).

Arc discharges are essentially the redistribution of charge. Since they involve the rapid motion of charged particles a transient electromagnetic signal is generated by the breakdown. This signal is referred to as electromagnetic interference, or EMI. EMI can induce undesired signals in electronic circuits, and also excite currents in the skin of the satellite which in turn can induce anomalous currents in internal satellite wiring. Both can cause satellite anomalies producing an unintended logic change in an electronic

system, or a spurious detector response. The electrical breakdown process produces localized heating and the evolution of material at the site of the arc. On sensitive satellite components, such as thermal control or optical surfaces, even minor physical damage can seriously degrade performance. These effects have been produced in laboratory simulations and inferred from orbital observations. [Ref. 2:p. 295-304, Ref. 7:p. 61-76, Ref. 8:p. 237-246]

Arc discharges have been well correlated to satellite anomalies by Shaw, Nanevicz, and Adamo [Ref. them]. An instrument designed to detect both satellite surface charging events and discharges occurring on the exterior of the satellite was flown on a synchronous altitude satellite. They observed two distinct types of discharges, the first occurs during energetic electron injection events, i.e. magnetospheric substorms, and are attributed to differential surface charging. The second is independent of geomagnetic activity, but is strongly spin synchronized and occurs throughout the satellite's orbit, most frequently at local dusk. During the time of the experiment, 35 anomalous events on the spacecraft were reported, 31 coinciding with recorded discharges. [Ref. 7:p. 61-76]

b. Deep Dielectric Charging

Deep dielectric, or bulk charging is the deposition of charge within the body of a dielectric. If the rate at which incident energetic electrons deposit in the bulk of a dielectric material exceeds the rate at which the charge leaks out due to the total conductivity (intrinsic conductivity plus radiation

induced conductivity), then a bulk charge and subsequent potential will build up. This can have deleterious effects on spacecraft systems. Foremost is electrical breakdown of the dielectric material.

Deep dielectric charging was first proposed as a discharge mechanism for dielectrics onboard spacecraft by Meulenberg [Ref. 8:p. 237-246]. He departed from the conventional belief that the discharge was through or between spacecraft surface components and proposed a bilayer discharge mechanism through the dielectric. This type of mechanism is able to explain many of the observed satellite anomalies that do not correlate with discharges induced by surface charging. When arc discharges were first associated with satellite anomalies, two distinct types, alluded to previously, were recognized: those that correlated with surface charging, and those occurring when surface charging was not a viable explanation [Ref. 7:p. 61]. Considerable work has since been done on the mechanism of electrical breakdown in irradiated dielectrics, and their association with anomalous satellite behavior.

Vampola summarized the viability of deep dielectric charging at synchronous altitude, and presented several definitive examples of this mechanism [Ref. 9:p 21-30]. The most common ailment associated with deep dielectric charging is the deposition of charge in the insulating covers on cables exposed directly to the space environment. When electrical breakdown is reached, a spurious signal occurs in the cable and thus in the connected

electronic component. Numerous cases of anomalous behavior attributed to deep dielectric charging have been identified [Ref. 10:p. 15-7, Ref. 11:p. 25-1, Ref. 12:p. 50].

Descriptions of radiation induced dielectric charging and discharge theory most useful to this thesis are by Wenaas concerning the order of magnitude calculations of dielectric charging in a high energy natural environment; by Fredrickson, and by Reagan et al. in an application of theory to observations from the SCATHA satellite [Ref. 13:p. 2281-4, Ref. 14:p. 337-343, Ref. 15:p, 386-412, Ref 16:p. 1-28, Ref. 17:p. 354-365]

The most complicated aspect of the dielectric charging process is the calculation of electron transport through the material resulting in a dose rates and charge distribution. Local dose rate is necessary to calculate the radiation induced conductivity which, combined with the intrinsic conductivity of the material, governs the leakage current. Electron transport is most accurately calculated through Monte Carlo calculations. The most definitive work in this area is that of M. J. Berger and S. M. Seltzer of the National Bureau of Standards in a fortran program, ETRAN. This work has evolved into the Tiger series of electron and photon transport code. Other Monte Carlo simulations exist, such as the AURORA code used by Reagan et al. [Ref. 17:p. 358], and POEM used by Beers et al. [Ref. 18:p. 209] TRW is currently developing a program, Deep Charging Analytical Technique (DCAT) that utilizes an algorithm developed by Tabata and Ito. [Ref. 19:p. 226-239, Ref. 20, Ref. 21]

3. Environmental Factors

Environmental factors affecting earth orbiting satellites are primarily the charged particle populations trapped by the earth's magnetic field. The geometry of the earth's magnetic field governs the structure of the particle populations, and the cavity in which they are contained is the magnetosphere. The geomagnetic field produces a semipermeable barrier to the flow of solar wind plasma and the resulting interaction produces a magnetic bubble, the magnetosphere, in interplanetary space (see Figure 1).

The magnetospheric radiation environment is distributed spatially by particle type, and by particle energy. The most common parameter used to characterize the magnetosphere is McIlwain's parameter L (McIlwain, 1961). The L values are derived from surfaces generated by the rotation of a dipole field about the earth's magnetic axis. The surfaces (field lines) are labeled by the distance from the center of the earth, in units of earth radii, to the minimum B (the magnetic equator), on that line. The inner zone is the region up to L = 2.5 and encompasses low earth orbits. The outer zone is the region beyond L = 3.0 out to the magnetopause, and encompasses geosynchronous orbits. The magnetopause is the "boundary" between the solar wind and the magnetospheric plasma. [Ref. 22:p. 341]

The predominant characteristics of the inner zone, from the point of view of spacecraft operations, are its relative stability, and intense high energy proton fluxes. These fluxes exceed 10^3 protons/cm^2-sec-sr for energies greater

than 50 MeV. The charge particle flux in the outer zone is much more variable. Both the electron and proton fluxes are strongly influenced by magnetic activity. Variations, dependent on local time, in particle populations at synchronous altitude (L>5) were first reported in a study of ATS-1 data [Ref. 23:p.5257-5264]. Enhanced particle fluxes were seen during periods of magnetic activity in the local midnight region of synchronous orbit. The postulated source of these observed particle populations was an influx of energetic plasma from the magnetospheric tail. These ideas were further refined by DeForest and McIlwain [Ref. 24:p.3587-3611]. Observations from ATS-5 reHxaled frequent injections of hot plasma into the synchronous orbit region of the magnetosphere. These plasma fluxes were found to have a one-to-one correspondence with magnetospheric substorms. Additionally, these injection events were found to insert a relatively discrete set of particles, referred to as a "plasma cloud", into the region. Those injections resulted in a second particle population superimposed on the preexisting ambient particle distribution (see Figure 2). These injection events can precipitate high levels of spacecraft charging, and are associated with the charging events on ATS-5 [Ref. 1:p. 653]. This sequence of events results in the well documented "midnight to dawn" period of high satellite anomaly activity (see Figure 3).

Other sources of hazardous radiation to spacecraft systems include cosmic rays and solar flare protons. The cosmic ray flux is on the order of $1/cm^2$-sec, and their interaction with spacecraft systems cause SEUs of

sensitive microelectronic devices and background noise in sensitive sensors systems. Energetic protons (E > 5 MeV) produced by solar flares can reach the earth within hours after a flare given the proper alignment of the interplanetary magnetic field between the sun and the earth. These particles have direct access to the magnetosphere over the polar caps and to synchronous orbits. The energetic proton fluxes may be as high as $10^5/cm^2$-sec-sr and produce dose rates in excess of 100 rad/hr. The radiation dose resulting from this intense exposure is extremely damaging to spacecraft subsystems such as solar cells, amplifiers and optical sensors. Spacecraft weight considerations have produced a tendency to use thinner exterior materials, such as glass solar cell coverslides. Thinner coverslides are less able to shield sensitive semiconductor material from radiation damage, conversely, the potential for spacecraft charging from thick dielectric charging increases with thickness of the dielectric. Thus optimum shielding thicknesses are obtained from balancing these two competing requirements. The energetic protons also produce SEUs. Energetic electrons are also produced by these events, but the additional fluxes are not significant in comparison to the existing electron population.

B. PURPOSE

Daylight charging of geosynchronous satellites is attributed to differential charging between shadowed insulators and conducting surfaces. Insulating surfaces in shadow can reach large negative potentials because of the lack of photoemission and the electrical resistance of the material. This differential charging can produce electrostatic barriers about the satellite which can suppress photoemission and secondary electron emission from the conducting surfaces. Under these conditions the entire satellite will charge to a negative potential [Ref. 25:p. 1313-1319]. Formation of a potential barrier was observed on ATS-6 [Ref. 25:p. 6809-6819]. Figure 4, a diagram of ATS-6 (which is 3-axis stabilized) shows that it will always have some surfaces in shadow for a substantial period of time.

Not all cases of spacecraft charging in sunlight can be attributed to shadowed insulating surfaces. ISEE1 is one in a series of three satellites which comprise the International Sun Earth Explorer project. The satellite is essentially a spin-stabilized cylinder (see Figure 5). Despite its lack of extensive shadowed surfaces, and its construction to electrostatic cleanliness specifications, significant charging events have been recorded on ISEE1. The satellite reached a negative potential on the order of -100 volts in sunlight as it transited the synchronous orbit region of the magnetosphere at 0300 LT on 17 March, 1978 [Ref. 27:p. 5568-5578]. Olsen et al. observed a potential barrier on the order of -10 to -20 volts with respect to the satellite body in

conjunction with this event [Ref. 26:p. 6809]. They also determined the barrier was not the result of space charge effects, and thus was most likely the result of differential charging of satellite surfaces. However, the spin rate of the satellite, 20 rpm, does not allow sufficient time for negative charge to build up on shadowed surfaces, (ignoring "ends"). The time constant of differential surface charging for dielectrics is on the order of a minute. [Ref. 28:p. 435] Thus from the standpoint of differential surface charging, the total charge on the surface of the satellite must always be greater than zero. This leaves no obvious explanation for the observed charging events of ISEE1 [Ref. 29]. It is important to identify this charging mechanism, and thus the overall expectation for the effectiveness of this type of electrostatic cleanliness measure.

This thesis will examine charging of exterior spacecraft dielectrics, and determine if sufficient charge can be deposited to produce differential charging of the dielectrics with respect to the spacecraft frame. These processes are illustrated in Figure 6. This occurs if the Gaussian pillbox in Figure 6 contains an overall negative charge. A net negative potential results, and potential barriers may form allowing the entire spacecraft to charge negatively. The formation of a potential barrier is illustrated in Figure 7, the "saddle point" corresponds to the potential barrier. This mechanism will be applied to the ISEE1 charging event. This thesis will show that the charging of exterior dielectrics is a viable mechanism for differential surface charging.

II. THEORY

A. SURFACE CHARGING

The equilibrium potential of a satellite will be such that the net current to the satellite surface is zero. This can be described by

$$(1) \qquad J_{PHOTO}+J_{SEC}+J_{BACKSCATTERED}-J_{AMB}=0$$

where

- J_{PHOTO} = the photoelectric current
- J_{SEC} = the ambient particle current
- J_{BS} = the backscattered electron current.

In general the net current to a sunlit satellite surface is positive for all magnetospheric plasma environments outside of L = 3. This is because the photocurrent is much larger than the ambient plasma currents (roughly an order of magnitude larger). In the absence of sunlight, the secondary electron emission can still balance the ambient electron current for low temperature environments [Ref. 30:p. 493].

The potential can be calculated from the simple relationship Q = VC, however in practice this is an extremely complicated process owing to the interrelationship between the currents and the potential. As a positive potential develops on the satellite, it modifies the current flow to the satellite surface. This process can be expressed simply as

$$2) \qquad J_{TOTAL} = (J_{PHOTO} + J_{SEC})\, e^{-\phi \frac{\phi}{KT}} + J_{BS} - J_{AMB} \qquad -$$

where KT is the characteristic temperature of the emitted photo and secondary electrons, and ϕ is the spacecraft surface potential. The energy of the backscattered electrons is high enough to ignore the effect of the developed potential.

As the satellite approaches equilibrium the potential develops such that the total current flow to the satellite surface goes to zero and equation (1) is satisfied. These calculations are complicated by several factors. For instance, the photoelectric current is zero for surfaces in shadow. The area of a satellite in shadow is dictated by the satellite geometry, the type of stabilization (spin or three axis), the satellite orbit, and the time of day and the time of year. The material characteristics of the satellite surface are also important. Aside from the gross differences between conductors and insulators, the photoelectric, secondary, and backscattered electron yields are material dependent. These and other factors combine to present a very complicated and fragile equilibrium state.

1. Photoelectric Emission

Photoelectric emission results from the interaction between incident photons and a surface. If the photon energy exceeds the work function of the surface material, and electron is emitted. The energy of the emitted electron

material. For spacecraft charging applications the enHxgy spectrum of electrons emitted due to solar radiation is characterized by a Maxwellian temperature of 2 eV. Saturation current densities (i.e. the maximum photoelectric current density emitted from a surface at normal incidence and zero potential) for many common spacecraft materials have been computed by Grard [Ref. 31:p. 171] and are shown in Table I. These values are only good to within a factor of 10 and vary not only with surface material, but also surface condition [Ref. 29].

2. Thermal Flux

The ambient plasma in the magnetosphere is generally described by one or more Maxwellian distributions, [Ref 32:p. 2]

$$(3) \qquad F_i(v) = \left(\frac{m_i}{2\Pi K T_i}\right)^{\frac{3}{2}} e^{\frac{-m_i v_i^2}{2KT_i}}$$

- n = number density of the ith species
- m = mass of the ith species
- T = temperature of the ith species
- v = velocity of the ith species
- k = Boltzmann constant
- F = distribution function.

The ambient particle flux to a surface is given by

$$(4) \qquad \Phi = \iiint n(\vec{v}\cdot\vec{n})\, F(\vec{v})\, d^3v$$

when solved this yields the thermal flux,

$$(5) \qquad \Phi = n\sqrt{\frac{kT}{2\Pi m}}$$

The ambient electron current density to the satellite can be written

$$(6) \qquad J_{AMB} = \sum n_i e \sqrt{\frac{kT_{e_i}}{2\pi m_e}} - \sum n_i e \sqrt{\frac{kT_{p_i}}{2\pi m_p}}$$

where e is the charge on an electron, T is the appropriate temperature, n is number density and m is mass.

3. Secondary Electron Emission

Secondary electron emission occurs when an electron impacts a surface. The incident electron may undergo one of three processes: reflection, true secondary emission, or backscattering. Reflection is generally only significant at very low energies, E < 10 Ev, and is generally negligible. Secondary emissions result from the impacting electron losing energy while in the material. Portions of this energy can then excite other electrons which may escape the material at low energy, similar to that of photoelectrons (about 2 eV) [Ref. 33:p. 1209]. The secondary electron yield, δ(E), is defined as the ratio between emitted-secondary, and incident primary electrons. Secondary

emission is an important process in spacecraft charging because for certain energy ranges and materials δ can be greater than 1. The following expression, generally attributed to Sternglass (circa 1950), provides a useful and accurate yield function

$$(7) \qquad \delta(E) = 7.4\delta_{max}\left(\frac{E}{E_{max}}\right)e^{-2\sqrt{\frac{E}{E_{max}}}}$$

[Ref. 34:p. 1138]. The material dependent parameters are defined as follows:

- E_{max} = the energy where δ has its maximum
- δ_{max} = the secondary yield at E_{max}.

Table II contains secondary emission parameters for various materials.

Backscattering refers to higher energy particles, E > 50 eV, which leave the surface at energies only slightly lower than that of the incident electron. Backscattered electrons are distinguishable from true secondary electrons by their greater emitted energies. A very useful form of the backscattered electron yield function is

$$(8) \qquad \delta_{BS}(E) = 0.1\left(1.0 - \frac{0.5}{E}\right)\left(\beta + e^{-\frac{E}{5.0}}\right)$$

where β is

$$(9) \qquad \beta = 10.0\left(1.0 - \left(\frac{2.0}{e}\right)(0.037Z)\right)$$

Z is the effective atomic number of the material, and E is in keV. This yield function is valid for E > 50 eV, for E < 50 eV δ_{BS} is equal to 0 [Ref. 35:p. 104-105].

Both secondary emission and backscattering occur for ion impacts, but the fluxes are two orders of magnitude less than for those from electrons and will thus not be considered in this work [Ref. 34:p. 1138].

B. DEEP DIELECTRIC CHARGING

Deep dielectric charging results from the deposition of charge within the body of a dielectric. The rate at which charge builds up in a dielectric is governed by the rate at which electrons are deposited, and rate at which they leak out of the dielectric. Thus total charge density depends on the balance of these two processes. The accumulation of charge in a volume is dictated by the continuity equation:

$$(10) \qquad -\frac{\partial \rho}{\partial t} = \nabla \cdot J_D + \nabla \cdot \sigma E \ ,$$

where J_D is the incident high energy electron current.

Wenaas solved as the one dimensional case for a slab of thickness d by approximating the divergence of J_D as

$$(11) \qquad \frac{J_1 - J_0}{d}$$

J_i is the current entering the slab and J_o is the current exiting the slab. In which case, assuming zero initial stored charge, the charge density as a function of time is:

$$(12) \qquad \rho = \frac{J_i - J_o}{d} \frac{\epsilon}{\sigma} (1 - e^{-\frac{\sigma}{\epsilon} t}) .$$

[Ref. 13:p. 2281].

1. Electron Deposition

In order to calculate the charge accumulated, the number of electrons stopped within the dielectric must be determined. Energetic electrons incident on a surface suffer energy loss and scattering and some are eventually absorbed by, (i.e. deposited within) the material. There are four types of interactions that can take place between electrons and matter: (1) inelastic collisions with atomic electrons, (2) inelastic collisions with atomic nuclei, (3) elastic collisions with atomic electrons and (4) elastic collisions with atomic nuclei.

Inelastic collisions are the primary means by which electrons lose energy in matter. An inelastic collision with a nucleus results in a pulse of electromagnetic radiation (bremsstrahlung). These radiative losses are generally more important for relativistic electrons. Inelastic collisions with atomic electrons often result in the excitation or release of atomic electrons as well as a resulting energy loss in the penetrating electron. The probability of each type of collision is calculated from scattering theory. [Ref. 36:p. 2-1,2-2]

The statistical nature of these processes results in charge and energy distributions along the depth of the material. The most accurate means of solving the problem of electron transport in matter is the Monte Carlo method. Berger and Seltzer have developed a Monte Carlo code to calculate the charge distribution of electrons in matter, and have compiled this data for many materials [Ref. 37:p. 1-169].

Several computer codes exist to solve electron transport, as mentioned previously. The algorithm developed by Tabata and Ito has been used extensively, however the author was unable to reproduce their published results with the algorithm, thus it was not used for this analysis. [Ref. 19:p. 226-239]

2. Dielectric Conductivity

It can be seen from equation (12) that the saturation threshold is proportional to the conductivity of the dielectric material. The time required to reach saturation is on the order of the relaxation time, $\tau = \varepsilon/\sigma$. [Ref 13:p. 2282]

The conductivity of a dielectric has two components, the intrinsic conductivity of the material and the radiation induced conductivity, (RIC). The total conductivity of the material can be written as $\sigma = \sigma_i + \sigma_r$ where σ_i is the intrinsic conductivity of the material and σ_r is the radiation induced conductivity.

a. Radiation Induced Conductivity

Radiation induced conductivity is related to the dose rate and two material dependent parameters as follows:

$$(13) \qquad \sigma_r = kD^{\Delta}$$

D is the dose rate, k is the coefficient of radiation induced conductivity, and Δ is a material dependent parameter between 0.5 and 1.0 [Ref. 38:p. 2532]. For most purposes setting $\Delta = 1.0$ provides sufficient accuracy. The constant k must be determined empirically, and has been for many materials, by as many researchers. Published values can vary over more than two orders of magnitude for typical materials. Wall et al. have provided a useful guide to this and other pertinent dielectric properties [Ref. 39:p. 569-591]. Table III contains k for several typical spacecraft materials.

(1) Dose Rate. Dose rate is the rate at which energy is deposited within a material from incident radiation. It is measured in units of rads per second. A rad is 100 ergs per gram. For materials with a low effective atomic number dose is directly proportional to the electron kinetic energy. A quantity, specific thickness (T_s), has been defined in terms of electrons/cm^2-Mev so that a dose profile independent of material and kinetic energy can be calculated. This curve is shown in Figure 8. [Ref. 36:p. 2.16]

Specific thickness is given by

$$(14) \qquad T_s = \frac{\rho x N_o}{T} \sum_i f_i \left(\frac{Z}{A}\right) \qquad \left[\frac{\bar{e}}{cm^2 \cdot MeV}\right]$$

where f_i is the weight fraction of the i^{th} element in the material,

$$(15) \qquad f_i = \frac{n_i A_i}{\sum_i n_i A_i}$$

Parameters are defined as follows:

- n_i = the number of atoms in the i^{th} element of the material
- x = the depth in the material in cm
- N_o = Avogadro's number
- T = electron kinetic energy in MeV
- ρ = material density in g/cm^3
- Z = effective atomic number
- A = atomic weight.

The dose profile for a low Z material is obtained by modulating the front surface dose with the curve in Figure 8. The front surface dose used is that for collisional stopping power. Collisions are the mechanism by which energy is deposited in the material, the energy from radiative stopping power is not deposited locally. Dose rate is obtained by multiplying the dose by the electron flux.

III. DATA

A. SOURCES

1. SCATHA

The SCATHA program, as mentioned, was a joint NASA/USAF project launched in 1979 to study spacecraft charging phenomena, and satellite response to it. Much of the experimental data used in this thesis was collected by instruments onboard the P78-2 (SCATHA) satellite. These instruments are the SSPM, SC3, and SC9. The next thrHx sections will provide descriptions of these instruments.

a. SSPM

The following description of the Satellite Surface Potential Monitor (SSPM) was taken from Mizera et al., 1980 [Ref. 40:p. 277]:

> The three SSPM instruments contained four electrostatic field meters designed to measure the potentials from material surfaces mounted at fixed positions above the sensors. Positive and negative currents flowing through the sample materials are collected on the metalized backing and sent to an electrometer circuit. All measurements are digitized, accumulated, and read out every second. The current and voltage data are accumulated for 1.0 and 0.25 sec, respectively.
>
> These insulating materials are typically 5 mil thick with aluminum backing the Kapton, Silver backing the Teflon, and in the case of the quartz fabric mounted on Teflon a hole was cut though the entire Teflon backing so that the electric field form the fabric would reach the sensor. The collecting area for the current was determined by the size of the sample. Two sizes of samples were flown on the SSPM payload. With the exception of Kapton, all samples were approximately 13 cm square. In addition to the

standard smaller samples, one Kapton sample approximately 29 cm square (SSPM-2) was flown to examine the scaling effects of charging.

b. SC3

The following description of Lockheed high-energy particle spectrometer, SC3, was obtained from Davidson, et al., 1988 [Ref. 41:p. 79]:

> The SC3 particle telescope [Reagan et al., 1981a] employs a 200-um-thick surface barrier silicon detector to analyze electron in the range 47-299 keV. Behind this is a stack of five 2-mm-thick surface barrier silicon detectors used to analyze electrons in the range 263-4970 keV. Spurious high-energy particles are mostly eliminated by a surrounding anti-coincidence plastic and phototube system and aluminum shielding. A tungsten shield is used to attenuate bremsstrahlung radiation produced by electrons within the region shielded by aluminum. The detection of electrons below 300 keV is unaffected by bremsstrahlung because of the low volume of the sensor. Above 300 keV the counting rates are moderately contaminated by bremsstrahlung, especially in the first energy above 300 keV; the bremsstrahlung contamination has been estimated and corrected for in the processing of the data. The particle type and energy range for analysis are uniquely established by specifying in the on-board instrument memory the coincidence/anticoincidence logic conditions and the gain and energy thresholds for the various sensor elements.

c. SC9

The following description of the SC9 UCSD Charged Particle Experiment was taken from The IMS Source Book, [Ref. 42:p. 73-78]:

> The instrument consists of five electrostatic analyzers, three for ions and two for electrons. Pairs of ion and electron analyzers are in rotating heads. One head is for low energies the other for higher energies. The third ion analyzer is a low energy unit mounted to view perpendicular to the spin axis. The rotating heads can rotate the analyzer fields of view over a range of angles (about 220 degrees) which includes both parallel and perpendicular to the spin axis. The two rotating heads scan in orthogonal planes.

This instrument provides the detailed plasma distribution function measurements over a reasonable period (16 sec for a spectrum), which is longer (314sec) if all pitch angles are to be covered. The sensor can also select any of the five outputs for connection via a filter to a broadband transmitter. This allows special operations in which rapid fluctuations in the particle fluxes can be followed.

2. 1979-053

1979-053 is the international designator of the satellite on which two other instruments that collected data used in this thesis flew. The instruments are the Charged Particle Analyzer (CPA) and the Spectrometer for Extended Electron measurements (SEE). Both instruments were provided by the Los Alamos National Laboratory.

a. CPA

The following description of the CPA was taken from The IMS Source Book, [Ref. 42:p 82-83]:

Each CPA consists of separate electron and proton sensor systems. The electron detectors are designated LoE (low-energy electron) and HiE (high-energy electron). LoE consists of a fan of five separate detector-collimator units at 0 degrees, +/- 30 degrees, and +/- 60 degrees to the spacecraft equatorial plane. The spacecraft rotate with a 10-s period about an axis points continually toward the center of the earth. Thus complete (over the unit sphere), continuous pitch angle measurements of the electron distribution are made by LoE each 10-s for essentially all magnetic field orientations. Each LoE sensor-collimator unit has a geometric factor of 3.6 x 10^{-3} cm^2-sr and is sensitive to electrons of energy between 30 and 300 keV (in 6 channels). The basic CPA sampling rate is 8 ms, so that each energy channel of each sensor is sampled 40 times per 10-s spacecraft rotation (i.e., 1200 total samples per rotation).

The HiE subsystem consists of a single detector-collimator unit that is pointed radially outward in the spacecraft equatorial (0 degree) plane. The HiE geometric factor is 1.8 x 10^{-2} cm^2-sr and its range of sensitivity is between 0.2 MeV and about 2 MeV. Since a single collimator unit sphere is sampled as the spacecraft rotates. For normal, approximately dipolar

magnetic field orientations nearly all pitch angles would be sampled by HiE, but for nondipolar (taillike) magnetic field configurations often encountered near midnight at 6.6 earth radii, very limited pitch angle sampling can result.

Both LoE and HiE have relatively thick aluminized mylar windows immediately in front of the sensitive solid state detector elements. This window eliminates contamination by sunlight, by very low energy (< 10 keV) electrons, and by protons below about 250-300 keV. Because of this feature, LoE provides a "clean" measurement of the 300 keV electron component, free of proton or low energy pileup contributions. In the case of HiE, the measurement relies on the soft spectral nature and low relative flux ratio of the > 300 keV proton (ion) component [Baker et al., 1979c] to effect the 0.2-2.0 MeV electron measurement in the presence of background ions.

b. SEE

The following description of the SEE was also taken from The IMS Source Book [Ref. 42:p. 83-84]:

The SEE combines thick solid state (dE/dx) detector elements with a bismuth germanate scintillator (total E) element to provide a new and unprecedented look at the very high energy electron component in the outer magnetosphere.

The energetic proton measurement at 6.6 earth radii is made by two separate CPA particle telescope systems: LoP and HiP. LoP is a single thin (about 40 um or 80 um on 1979-053) surface barrier solid state detector in front of an anticoincidence scintillator element. A sweep magnet is part of the LoP collimation system and eliminates <0.5 coincidence scintillator cup. HiP also has strong a sweeping magnet to eliminate contamination by < 1.0 MeV electrons. The High-energy proton telescope measures protons between 0.4 and 150 MeV in 16 quasilogarithmic differential energy channels with a geometric factor of 4.4×10^{-2} cm^2-sr (about 8×10^{-2} cm^2-sr for EP> 25 MeV).

3. ISEE-1

a. LEPEDEA

The following is a description of the LEPEDEA high energy electron spectrometer [Ref.27:p. 5569]:

> The University of Iowa LEPEDEA, is a quadrispherical detector, divided into 7 segments to cover the polar angle. This detector covers a 6° x 38° solid angle. During periods of low bit rate telemetry the detector covers the 200 eV to 45 keV energy range in 32 steps [Frank et al., 1978].

b. MEPI

The following is a description of the MEPI electron spectrometer [Ref. 27:p. 5569]:

> The Medium Energy Particles Instrument (MEPI) cover the 20 -1200 keV energy range with 8 channels in low bit rate. The detectors provide an angular resolution of 10° x 45° at low bit rate including spin and scan platform. Energy resolution is ~ 5%, with a geometric factor of 10^{-2} cm^2 sr.

IV. RESULTS

A. ISEE1 CHARGING EVENT

As discussed previously, ISEE1 is a spin stabilized, cylindrical satellite. All exterior surfaces, with the exception of the center, or "belly band" region housing the satellite instruments, are covered with solar cells (Figure 5). The solar cells are protected by silicon glass (SiO_2) cover slides, a dielectric material. The belly band region consists primarily of aluminum, a conductor. Thus the scenario exists for differential surface charging between conducting and insulating surfaces, however the satellite's high spin rate (20rpm) and lack of extensive shadowed surfaces preclude conventional differential charging mechanisms. It must be assumed that the electrostatic cleanliness measures adopted on ISEE1 were not completely effective, since the satellite charged. Electrostatic cleanliness was to be achieved by coating the entire satellite with a conducting material, indium oxide. This coating appears to have been largely effective. The problem area appears to have been a breakdown in the grounding of the oxide surface to the body, leaving the cover slide surfaces floating.

1. Charging Environment

The charging environment encountered by ISEE1 as observed by the LEPEDEA and MEPI instruments can be described by three essentially discrete populations. The lower energy spectrum (below 1 keV) has a Maxwellian density of roughly 3.7×10^5 electrons/m^3 and a plasma temperature of 314 eV. The keV electrons are characterized by a Maxwellian density of approximately 2.0×10^5 electrons/m^3 and a plasma temperature of 8.0 keV. These are values typical of the plasma sheet. [Ref. 27:p.5573] The higher energy spectrum (100 to 300 keV) is higher than typically observed in this region and was found to roughly follow an inverse power law of E^{-3}. The DST index is plotted in Figure 9 for several days prior to the observed charging event. Several substorms are apparent. ISEE1 is not in geosynchronous orbit, it merely transits this region of the magnetosphere twice during an orbital period. It therefore is only subjected to the geosynchronous environment for about an hour per transit.

Surface charging currents associated with this plasma environment are shown in Table IV. Figure 10 is a sample of the ISEE1 data used for calculations in following sections. Since differential flux is a function of both energy and angle, [$J(E,\alpha)$], a pitch angle of 90° was chosen as appropriate for this analysis. However, the flux varies as much as a factor of 10 over pitch angle (see Figure 11). Since trapped fluxes ($\alpha = 90°$) are at the minimum in

the pitch angle distribution, this choice provides a lower bound on the differential flux.

2. Mechanism Criteria

In order to attribute the ISEE1 charging event to the deposition of charge within the body of exterior dielectrics, the following condition must be satisfied:

$$(16)\quad \int_{T} J_E dt + \int_{\frac{P}{2}} (J_{AMB} - J_{SEC} - J_{BS})\, dt > \int_{\frac{P}{2}} (J_{PHOTO} + J_{SEC} + J_{BS} - J_{AMB})\, d$$

The variables are defined as follows:

- J_E = energetic (penetrating) electron current density
- J_{AMB} = ambient plasma current density
- J_{PHOTO} = current density from photoelectric emission
- J_{SEC} = current density from secondary electron emission
- J_{BS} = current density from backscattered electrons
- P = the spin period of the satellite, 3 secs.
- T = period of elevated energetic electron populations prior to the charging event, approximately 1 hour

Here J_{AMB} must be greater than $J_{SEC} + J_{BS}$ in order for there to be net negative charging or shadowed surfaces. This is the limiting case for zero potential. While the satellite is positive, terms such the photocurrent are substantially reduced. The solution of the integral J_E dt is equation (12) so that the total deposited charge density is given by:

$$(17) \qquad \int_T J_{Bdt} = J_B \frac{\epsilon}{\sigma}(1-e^{-\frac{\sigma}{\epsilon}}) \quad at\ t = T$$

3. Charge Deposition in the Coverslides

The solar cell slide cover slides on ISEE1 were made of 0.03 cm thick Corning 7940 industrial grade fused silica [Ref. 43:p. 2-3]. The energy range of electrons that would deposit within the body of the slide was determined to be roughly 100 to 200 keV. Electron penetration depth versus energy is shown for SiO_2 in Figure 12 This range was determined from tabulated values of electron penetration depths for Corning 7740 industrial grade fused silica [Ref. 37:p. 123]. While the 7740 glass does not have the same composition as the 7940 glass, negligible error should be introduced in the electron penetration depths. The primary difference between these glasses is the 7740 is less "pure", that is to say it has been doped. The effective atomic number and atomic weight are essentially unchanged. From equation (14) it is apparent these are the critical parameters in material stopping power. [Ref. 44:p. 16]

The intrinsic conductivity of Corning 7940 glass is $\sigma_i = 1x10^{-15}\ (\Omega\text{-m})^{-1}$, the dielectric constant, k = 3.8 [Ref. 44:p. 16]. Conductivity is a function of temperature, as shown in Figure 13. The goal of thermal control systems onboard spacecraft is to achieve an operating environment suitable for the instruments. The vast preponderance of scientific instruments operate in a temperature region near 25°C, and this value will be adopted for the surface

temperature. The effect of radiation on the conductivity was considered. Radiation induced conductivity (RIC) was calculated from equation (13). The dose rate used was the maximum dose averaged over the thickness of the sample. A summary of these calculations is provided in Table IV.

4. Summary of the ISEE1 Charging Results

Data from the ISEE1 charging event, and several variations of this data, were applied to equation (16). Table V is a summary of these results. The effect of radiation induced conductivity was taken into account. This effect resulted in about a 20% to 25% reduction in the deposited charge densities. The calculations show that for the ISEE1 data set this mechanism does not produce sufficient deposited charge to result in differential charging of the satellite. However, an order of magnitude increase in the high energy (100-200 keV) electron flux does result in negative charge on the dielectric. This is within the accepted range of the 100 to 200 keV electron flux measurements. It is also appropriate for the uncertainty associated with the photoelectric current. An order of magnitude decrease in the photoelectric current would be necessary to create conditions in which the deposition of charge in the cover sides would be sufficient to produce differential charging of the satellite for our 90° pitch angle measurements of the ambient spectra.

The energetic fluxes observed in conjunction with the ISEE1 charging event are by no means extreme values for the geosynchronous substorm environment. Reagan et al. (1983) reported energetic flux (100 to 300 keV)

values during magnetic storms, and substorms that were as much as 2 orders of magnitude greater than the ISEE1 fluxes (see Figure 14). It appears that it is then possible for net negative charge to be established, and hence differential charging induced barriers can form.

B. MATERIAL RESPONSE

Surface potential measurements are made by the SSPM instruments onboard the SCATHA satellite for several common spacecraft materials. Trends in these potentials for two materials, Teflon and Kapton, were measured during a period of magnetospheric activity, and will be compared to calculated deposited charge densities. These materials are of interest because both are used extensively as spacecraft thermal control surfaces.

1. Charging Environment

The time period from day 160 to 170 (Julian dates), 1980, was identified by Baker et al.(1984) as one of intense magnetospheric activity characterized by elevated energetic electron fluxes. Extremely high flux levels for very energetic electrons (2 to 7 MeV) were recorded. [Ref. 45:p. 9] The DST index is plotted in Figure 15 for this period. Unfortunately the energetic (30 to 100 keV) electron flux data for this period was unavailable at the time of this writing. However elevated energetic electron flux levels can be inferred from the DST index alone. For calculational purposes the flux levels recorded by the ISEE1 instruments will be used.

2. Sample Characteristics

The calculations made for the ISEE1 cover slides were repeated for both the Teflon and Kapton samples. The thickness of both SSPM samples is 127μm. The energy range of electrons that would deposit within each sample was found to be:

- Teflon 35 to 125 keV
- Kapton 35 to 100 keV

The electron penetration range versus energy is shown for both Teflon and Kapton in Figures 16 and 17 respectively. Comparison to the penetration depth of energetic electrons in SiO_2 (Figure 11) reveals that a much lower range of electron energies deposit within the body of these two dielectrics. In terms of spacecraft charging, this means that Teflon and Kapton are vulnerable to charge deposition from electrons with energies characterized by much higher ambient flux levels than those affecting SiO_2. Table VI summarizes the results of these calculations; the SiO_2 results are repeated for comparison.

The saturation values for deposited charge were calculated because SCATHA is a geosynchronous orbit satellite and thus is subjected to elevated electron flux levels for longer periods of time than ISEE1. It can be concluded from the DST index that the magnetic storm activity for this period exceeded the material time constant, τ, in each case. In two cases (the intrinsic conductivity values of both SiO_2 and Teflon) the saturation charge exceeds the commonly accepted charge threshold value of 1.6×10^{-3} C/m^2 for dielectric

breakdown. Should dielectric breakdown be reached, arcing will occur, but arcing does not remove a significant amount of the bulk charge. An equilibrium is established such that bulk charge remains below the threshold value.

Radiation dose rates calculated were on the order of 2 rads/sec for Teflon and Kapton. RIC for Kapton was not significant. These results are consistent with those obtained by Reagan et al. [Ref. 46:p. 74].

3. Summary of Results

The surface potential of each material is plotted at 0700LT for each day in the aforementioned period in Figures 18 and 19. The potentials were measured at a single local satellite time to eliminate some of the daily variations to be expected at geosynchronous orbit. Teflon exhibited a trend towards an increasingly negative potential. The Teflon surface potential became more negative by approximately 440 V. The Kapton sample retained a fairly constant value of -25 V (relative to the spacecraft mainframe) throughout this period. The Teflon measurements are qualitatively consistent with the values in Table VI. The Kapton results, however are more difficult to explain.

Using the simple relationship $Q = VC$, and a capacitance of $100 pF/m^2$ (considered standard for spacecraft surfaces [Ref. 47]), the accumulated charge densities calculated for Teflon can easily account for the observed change in potential. For example, the smallest accumulated charge density for Teflon is

$2.4x10^{-5}$, which yields a potential of 240 kV. Of course, this high of a potential would never be reached because electrical breakdown would occur at a much lower potential. The effect of the surface currents (J_{SEC},J_{BS}, and J_{AMB}) has not been included and these will of course greatly modify the surface potential.

The constancy of the Kapton sample's voltage throughout the period studied indicates that this is its equilibrium voltage for the environmental conditions encountered. The voltage is much less negative than the values of deposited charge in Table VI would indicate. Kapton has a much higher intrinsic conductivity than either Teflon or SiO_2, and subsequently a much smaller value of τ. This characteristic coupled with the effect of the surface currents may explain the observed potential, but seems unlikely to the author. If this were the case, then extremely large potentials would never be expected on Kapton, yet a differential potential of -2100 V was recorded on the SCATHA SSPM Kapton sample during a substorm event in March of 1978 [Ref. 46:p 81].

Energetic electrons of energies ranging from roughly 1 to 200 keV have been associated with spacecraft surface charging phenomena by Reagan et al. for SCATHA [Ref. 46:p.74-85]. Mullen et al. (Feb 1986) did a correlation analysis on the total electron flux and levels of the frame potential for several SCATHA charging events. They concluded that the high-energy portion of the electron flux drives spacecraft charging. The strongest correlation was to the 58.3 keV instrument channel, encompassing the energy range 30 to 75 keV. Additional correlation was found from the 23.8 keV channel up to the 335 keV

channel, depending on the day presented. These results are shown in Figure 20. The primary concern in Mullen's work was surface charging, however these energy ranges also correspond to enhanced dielectric charging. This work suggests that the correlation between the daylight charging events observed on SCATHA and intense 50 -100 keV electron fluxes may be partially due to deep dielectric charging. [Ref. 48:p. 1484-85]

V. CONCLUSIONS

Energetic electrons (keV electrons) play a definite role in spacecraft charging. The precise role of a given energy ranges depends on material. The energy range from 30 to 100 keV was found to be the energy range at which electrons will deposit within a dielectric such as Kapton, or Teflon. Fused silica required a harder energy spectrum for penetration, 100 to 200 keV.

Qualitatively, electron deposition within the bulk of exterior dielectrics as a mechanism capable of producing spacecraft charging has been demonstrated. Energetic (10-100 keV) electrons deposit within exterior dielectrics, and have a substantial lifetime within these dielectrics. The deposited negative charge can eventually exceed the positive charge left by the electron flux departing the surface as a result of photo, secondary, and backscattered electron emissions. The results in Table V support this mechanism as the cause of the ISEE1 charging event if the higher values for energetic electron fluxes are used. The electron flux data, and calculated flux values used in thesis are accurate to an order of magnitude (J_E, J_{PHOTO}, J_{AMB}, etc.). Variations reflecting these approximations are included in Table V, and demonstrate that the deposition of electrons within exterior dielectrics can be the dominant process in environments not uncommon to geosynchronous orbit.

The mechanism appears to be general and will be important on most synchronous altitude satellites.

Further work is recommended in several areas. First, it is recommended that a computer simulation be used to determine the charge and energy deposition distributions within the dielectric as a function of depth. The energy ranges used in this thesis to calculate the deposited charge were restricted to specific ranges, future work should apply deposition algorithms to the entire energy spectrum to which the spacecraft is exposed, specifically the energy range below 1 keV should not be neglected. From this information electric fields, conductivities, and thus leakage currents within the dielectric can be much more accurately determined. Second, another computer simulation, to model the satellite potential as a function of time, is necessary. To properly understand this mechanism, one needs to study how the satellite reaches its equilibrium potential as it is dictated by all the discussed surface phenomena (photoelectric effect, secondary electrons, etc.) as well as the impact of deposited charge. An attempt was made to program the aforementioned phenomena but was met with some difficulty. Finally, the mechanism needs to be thoroughly tested against in situ flux and potential measurements.

APPENDIX A

TABLE I

EXPERIMENTAL DATA ON PHOTOEMISSION

[Ref. 31:p. 171]

MATERIAL	SATURATION CURRENT DENSITY [μAm^{-2}]
Indium Oxide	30.0
Aluminum Oxide	42.0
Gold	29.0
Aquadag	18.0
Average	21.0

TABLE II

SECONDARY EMISSION PARAMETERS

[Ref. 29:p. 1210, Ref. 30:p. 1138]

MATERIALS	E(max)	δ(max)
Gold	800eV	1.45
Aluminum	300eV	0.97
Silicon Dioxide	420eV	2.50
Aquadag	350eV	0.75
Teflon	200eV	3.00
Kapton	150eV	2.10

TABLE III

COEFFICIENTS OF RADIATION INDUCED CONDUCTIVITY

UNITS [SEC/OHM-CM-RAD] [Ref. 35:p. 580]

MATERIAL	K_{max}	K_{min}
Kapton	$6x10^{-18}$	$1.2x10^{-19}$
Teflon	$1x10^{-16}$	$2x10^{-18}$
Mylar	$2.1x10^{-19}$	$1.8x10^{-19}$
Polyethylene	$4.5x10^{-18}$	$3x10^{-19}$
Polystyrene	$1x10^{-16}$	$2x10^{-18}$

TABLE IV

ELECTRON FLUXES ENCOUNTERED BY ISSE1 ON DAY 76 1977

CURRENT SOURCE	FLUX [$e/m^2 \cdot sec$]	CURRENT DENSITY [$C/m^2 \cdot sec$]
Photoelectric	1.311×10^{14}	2.098×10^{-5}
Ambient	3.667×10^{12}	5.867×10^{-7}
Secondary	2.778×10^{12}	4.445×10^{-7}
Backscattered	5.005×10^{11}	8.008×10^{-8}
Energetic	7.67×10^{9}	1.23×10^{-9}

TABLE V

ISEE1 SiO_2 RESULTS

ENVIRONMENTAL CONDITIONS	$Q_{energetic}$ [c/m^2]	Q_{shadow} [c/m^2]	$Q_{energetic} + Q_{shadow}$ [c/m^2]	Q_{sun} [c/m^2]
ISEE1 DATA $N=N_m$ $J_e=J_{Em}$	3.143×10^{-6}	9.312×10^{-8}	3.236×10^{-6}	3.138×10^{-5}
Modified ISEE1 DATA $N=10N_m$ $J_e=J_{Em}$	3.143×10^{-6}	9.312×10^{-7}	4.075×10^{-6}	3.054×10^{-5}
Modified ISEE1 DATA $N=N_m$ $J_e=10J_{Em}$	3.143×10^{-5}	9.312×10^{-8}	3.144×10^{-5}	3.138×10^{-5}
Modified ISEE1 DATA $N=10N_m$ $J_e=10J_{Em}$	3.143×10^{-5}	9.312×10^{-7}	3.228×10^{-5}	3.054×10^{-5}

$N \equiv$ plasma electron density [$\bar{e}$/m^3]

$N_m \equiv$ plasma density measured by ISEE1

$J_E \equiv$ energetic (E = 100 to 200 keV) electron flux

$J_{Em} \equiv$ energetic current density measured by ISEE1 instruments

$Q_{energetic} = J_E \, \varepsilon/\theta \, (1 - \beta^{-\theta/\varepsilon\tau})$

$Q_{shadow} = \int (J_{amb} - J_{SEC} - J_{BS}) \, dt$

$Q_{sun} = \int (J_{photo} + J_{SEC} + J_{BS} - J_{amb}) \, dt$

TABLE VI

SSPM AND SiO_2 RESULTS

MATERIAL	DIELECTRIC CONSTANT	$\tau=\varepsilon/\theta$ [Secs]	Q_{SAT} [c/m^3]	PENETRATING FLUX [c/m^2-sec]
SiO_2 (Corning 7940)				
- intrinsic	3.8	3.363×10^{4}	4.14×10^{-3}	1.23×10^{-7}
- RIC_{max}	3.8	4.931×10^{3}	1.24×10^{-4}	
- RIC_{min}	3.8	***		
Teflon				
- intrinsic	2.1	1.859×10^{5}	4.79×10^{-3}	2.58×10^{-8} c/m^2-sec
- RIC_{max}	2.1	929	2.40×10^{-5}	
- RIC_{min}	2.1	4.646×10^{4}	1.20×10^{-3}	
Kapton				
- intrinsic	3.0	2.66×10^{3}	6.68×10^{-5}	2.51×10^{-8}
- RIC_{max}	3.0	***		
- RIC_{min}	3.0	***		

*** In these cases the additional conductivity introduced due to radiation is not significant with respect to the intrinsic conductivity of the material.

* These values exceed the commonly accepted breakdown threshold for dielectrics of 1.6×10^{-3} c/m^2.

APPENDIX B

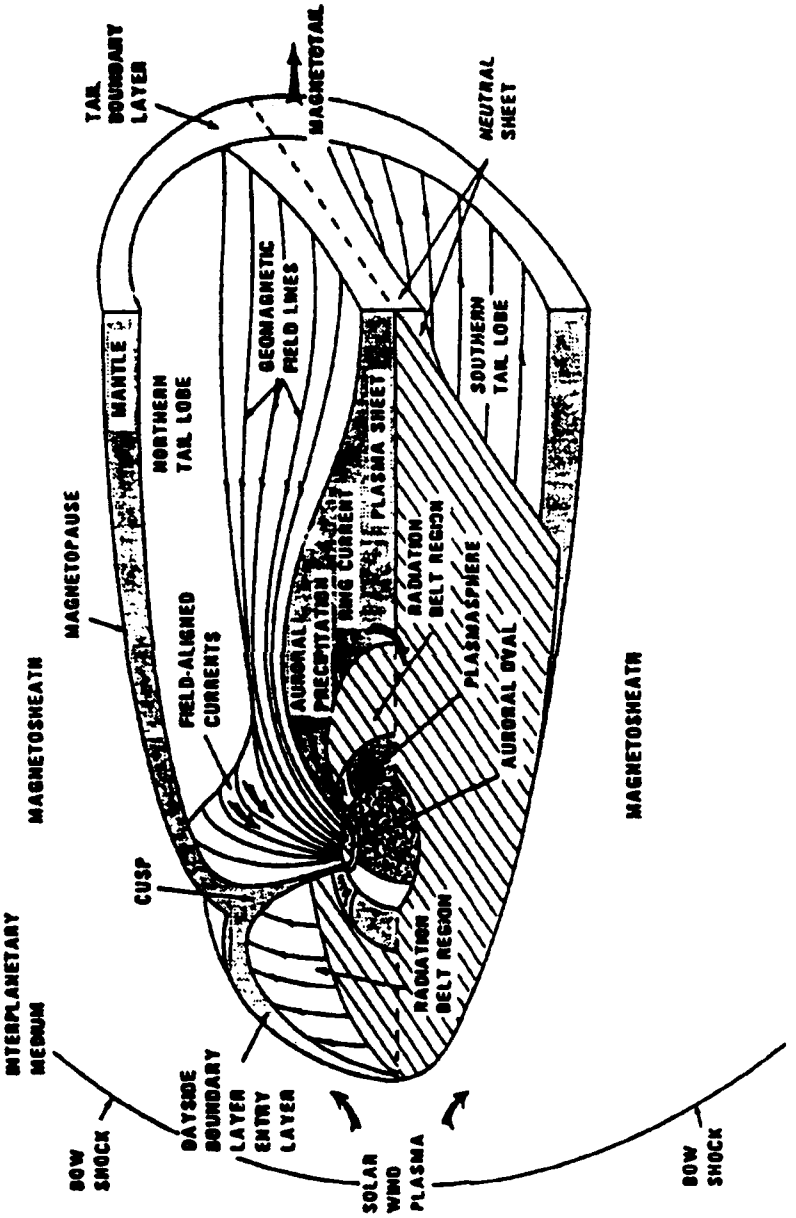

Figure 5.1 Cross section of the magnetosphere. For a quiet magnetosphere, geostationary altitudes are between the plasmasphere and plasma sheet (nighttime), and between the plasmasphere and dayside boundary layer (daytime). During active geomagnetic periods, geostationary satellites may become engulfed by the inward moving nighttime plasma sheet, and may pass through the daytime boundary (entry) layer *(after National Research Council, 1981)*.

Figure 1
The Magnetosphere
[Ref. 49:p. 46]

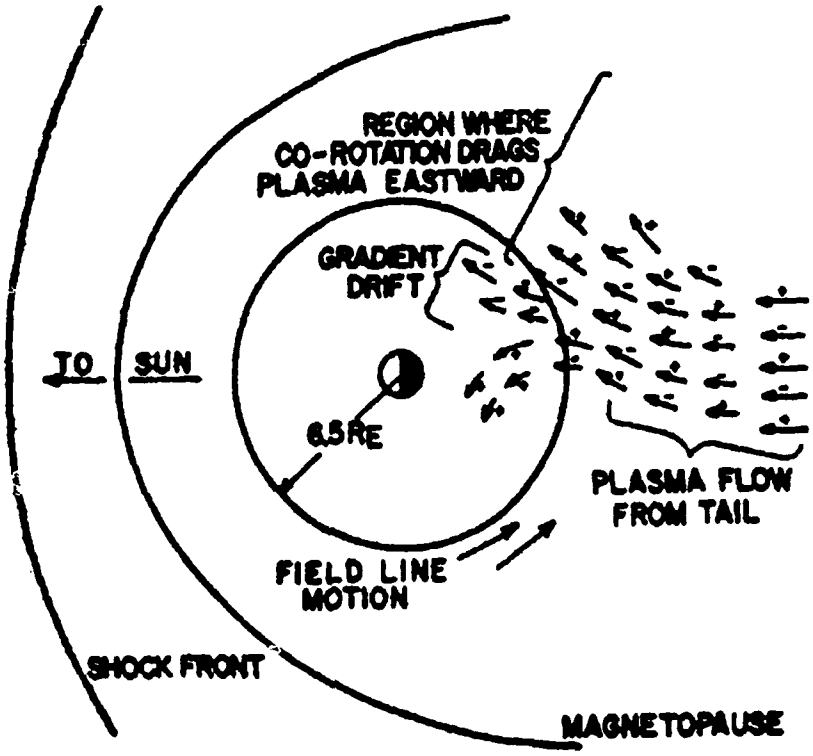

Fig. 6. A diagrammatic representation of the flow of plasma in from the tail showing the region where the plasma is swept eastward by co-rotation and, farther in, the region where curvature and gradient drift establishes the ring current through enhanced particle energies.

Figure 2
A Plasma Injection Event
[Ref. 23:p. 5263]

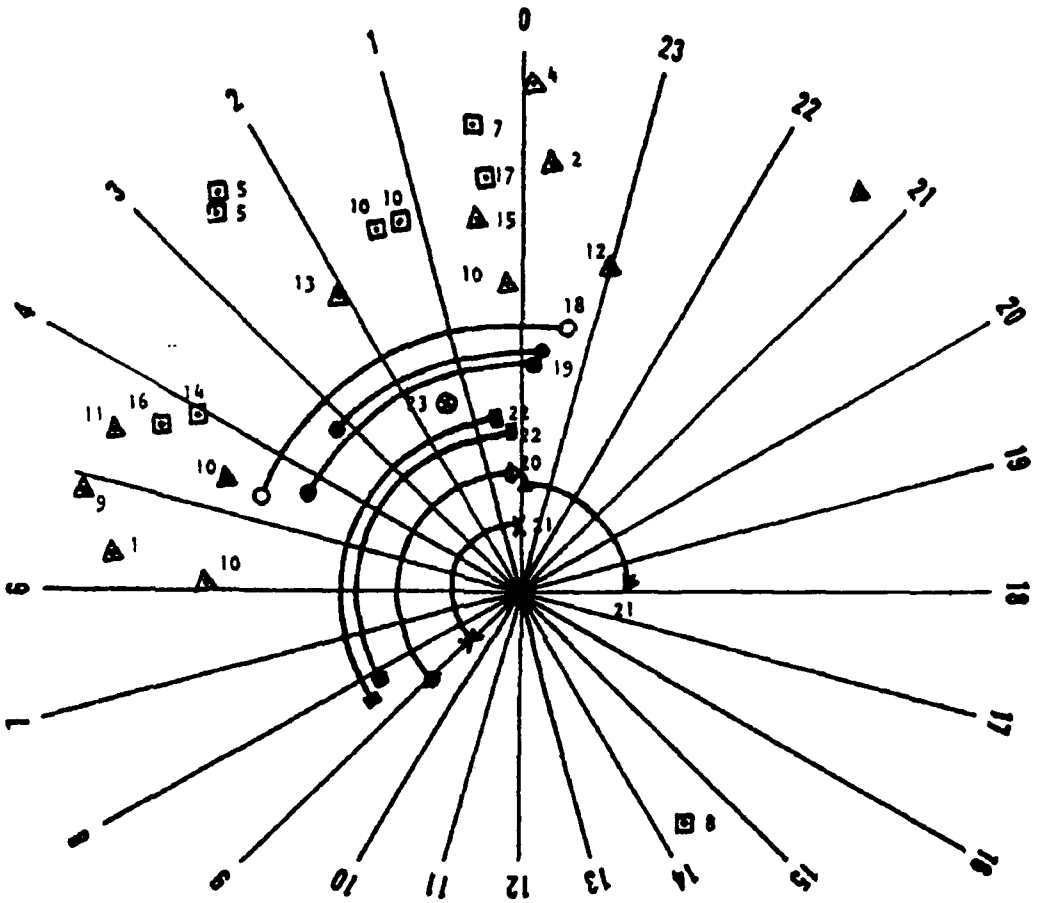

Fig. 1. Distribution of anomalies observed by several geostationary satellites. Rays are local time at spacecraft in hours, numbers identify events. Radius vectors have no significance, and differ only to allow visual resolution of events.

Figure 3
"Midnight-to-Dawn" Satellite Anomaly Pattern
[Ref. 2:p. 278]

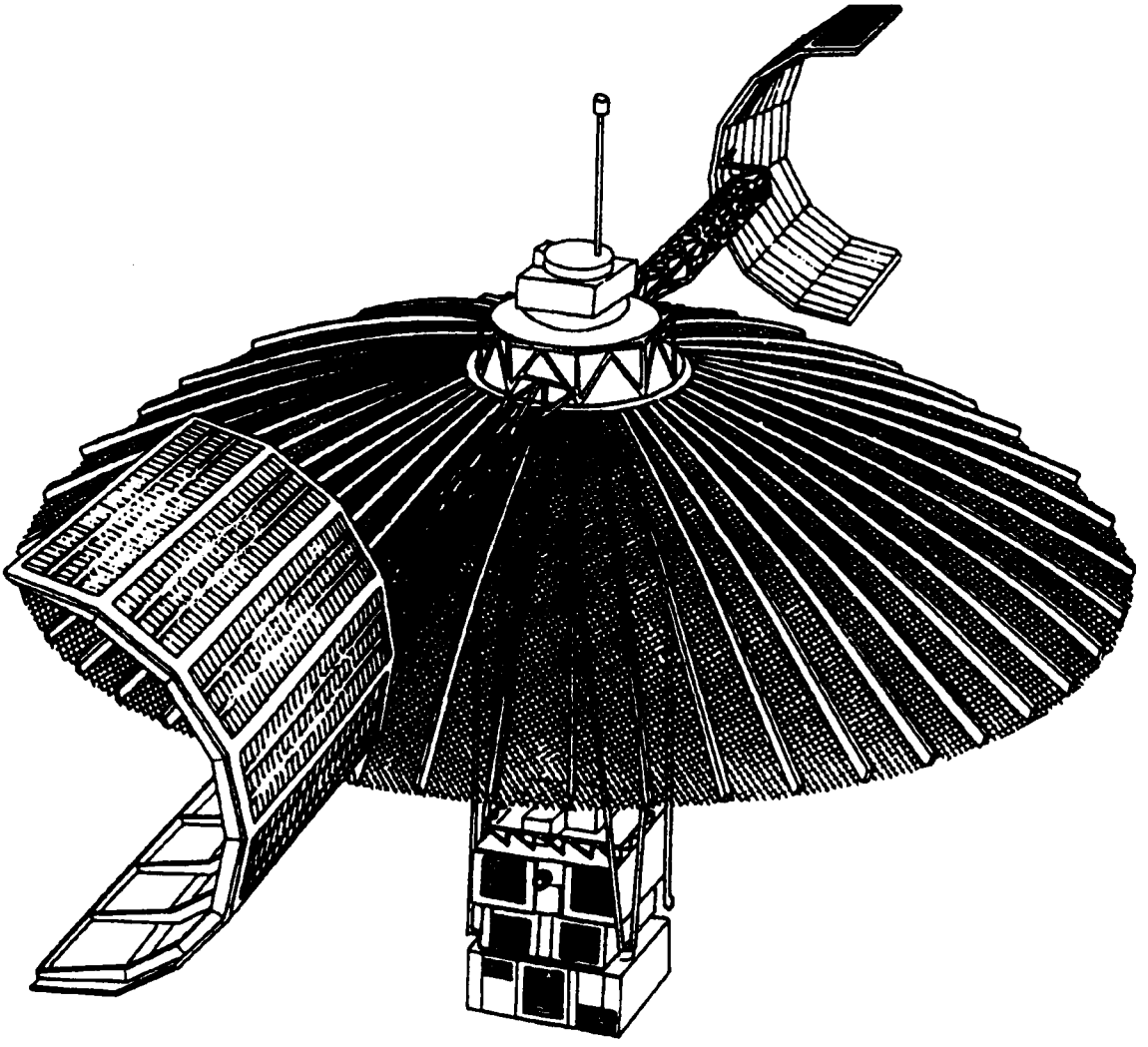

Figure 4
ATS - 6
[Ref. 50:p. 70]

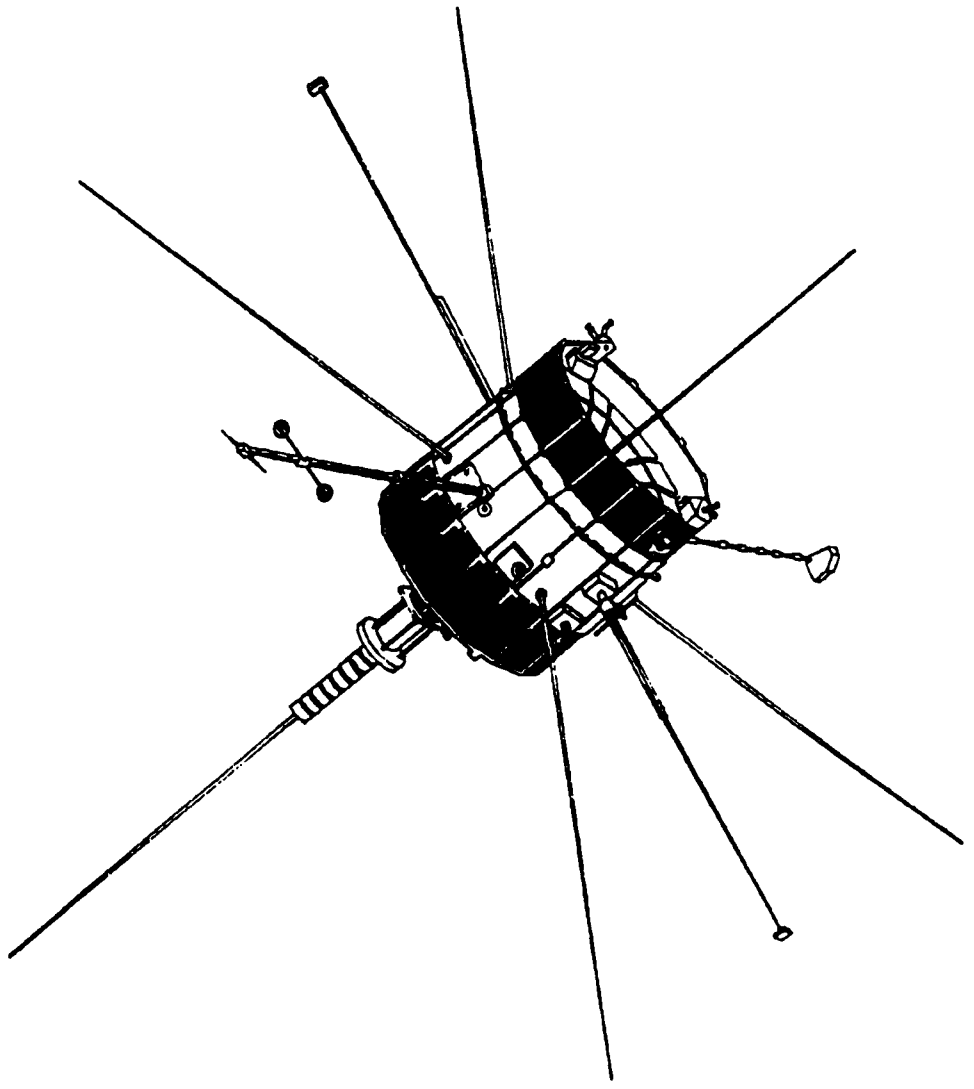

Figure 5
ISEE - 1
[Ref. 50:p. 151]

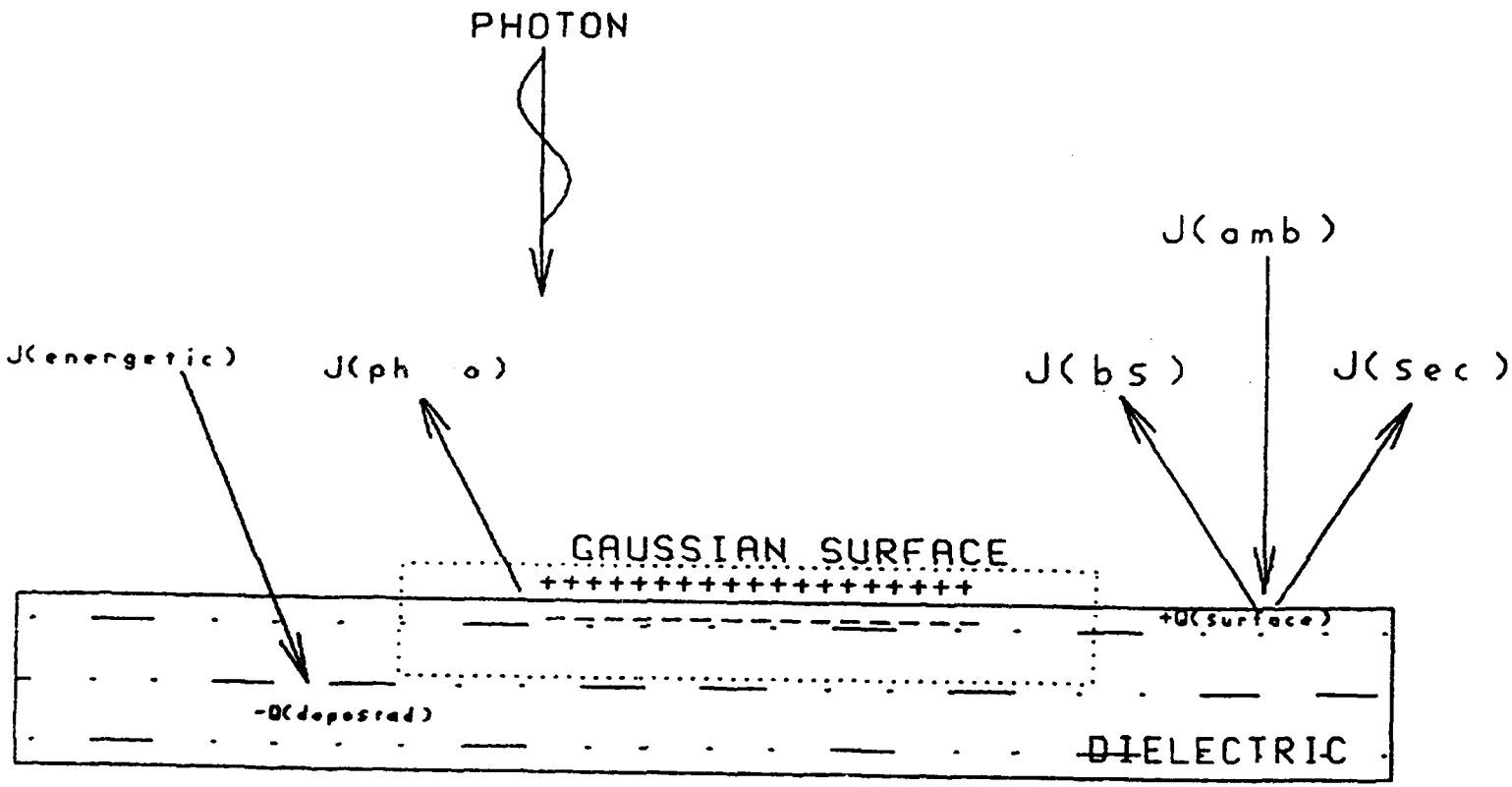

Figure 6
Spacecraft Charging Processes

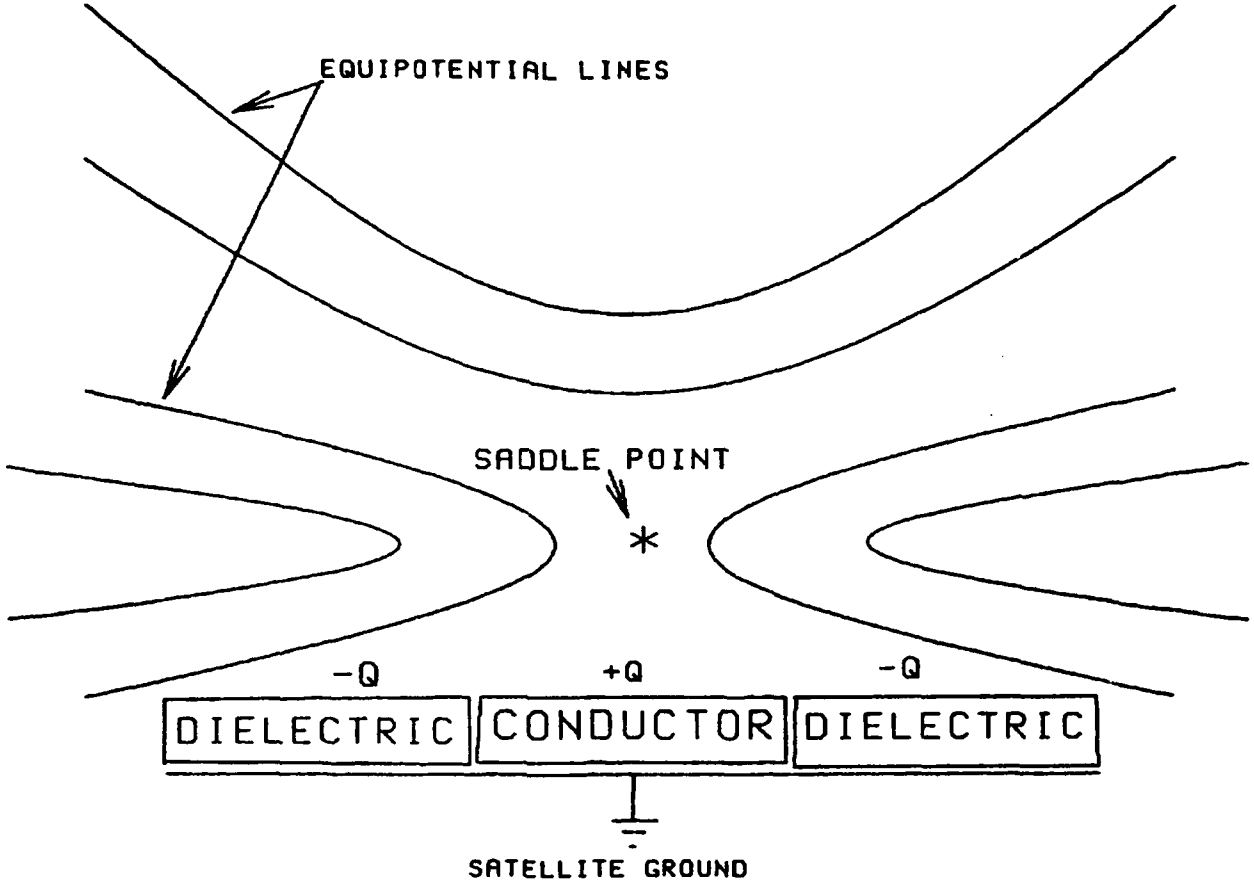

Figure 7
Potential Barriers

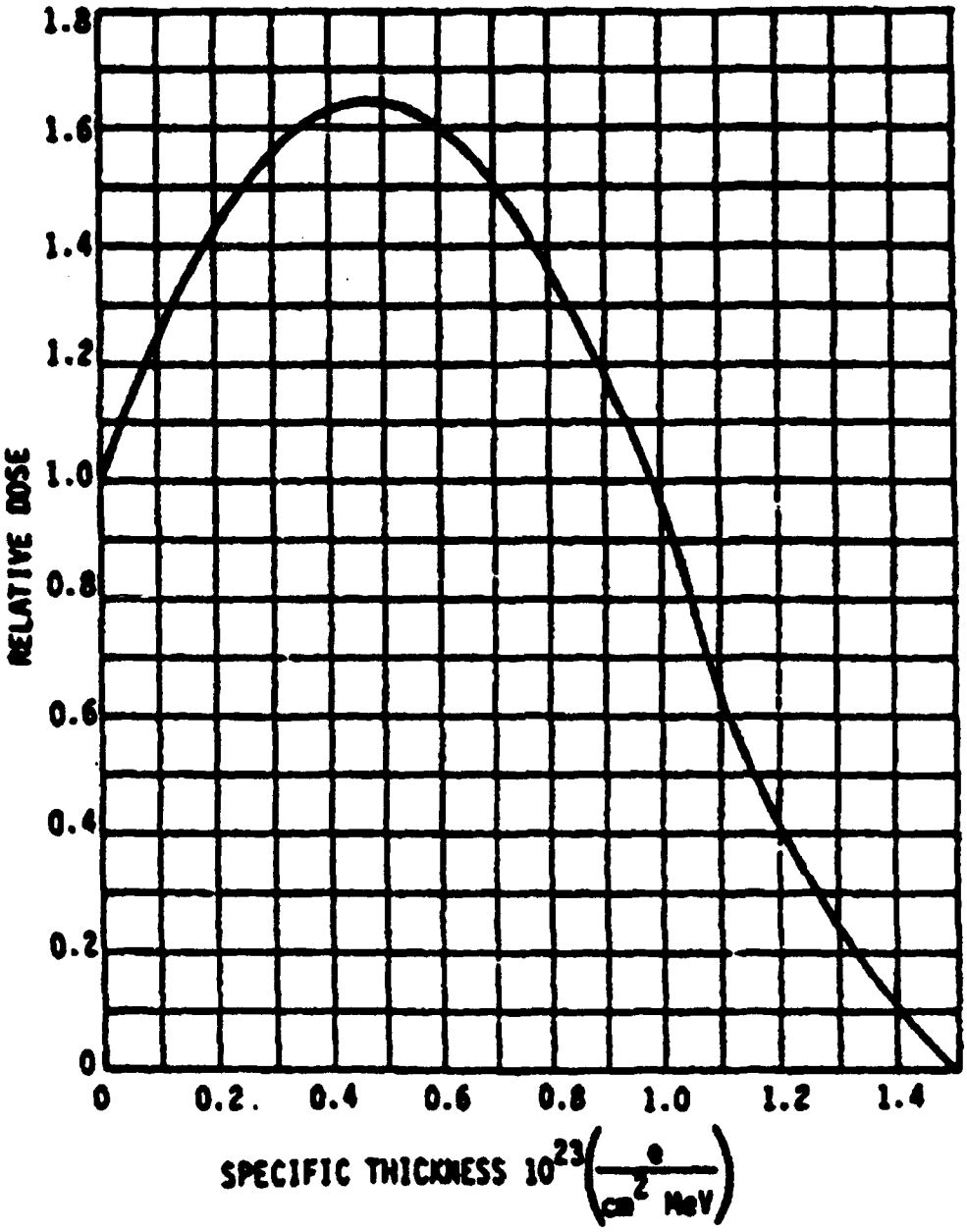

Figure 8
Electron Dose Profile in a Low-Z Material
[Ref. 36:p. 2-16]

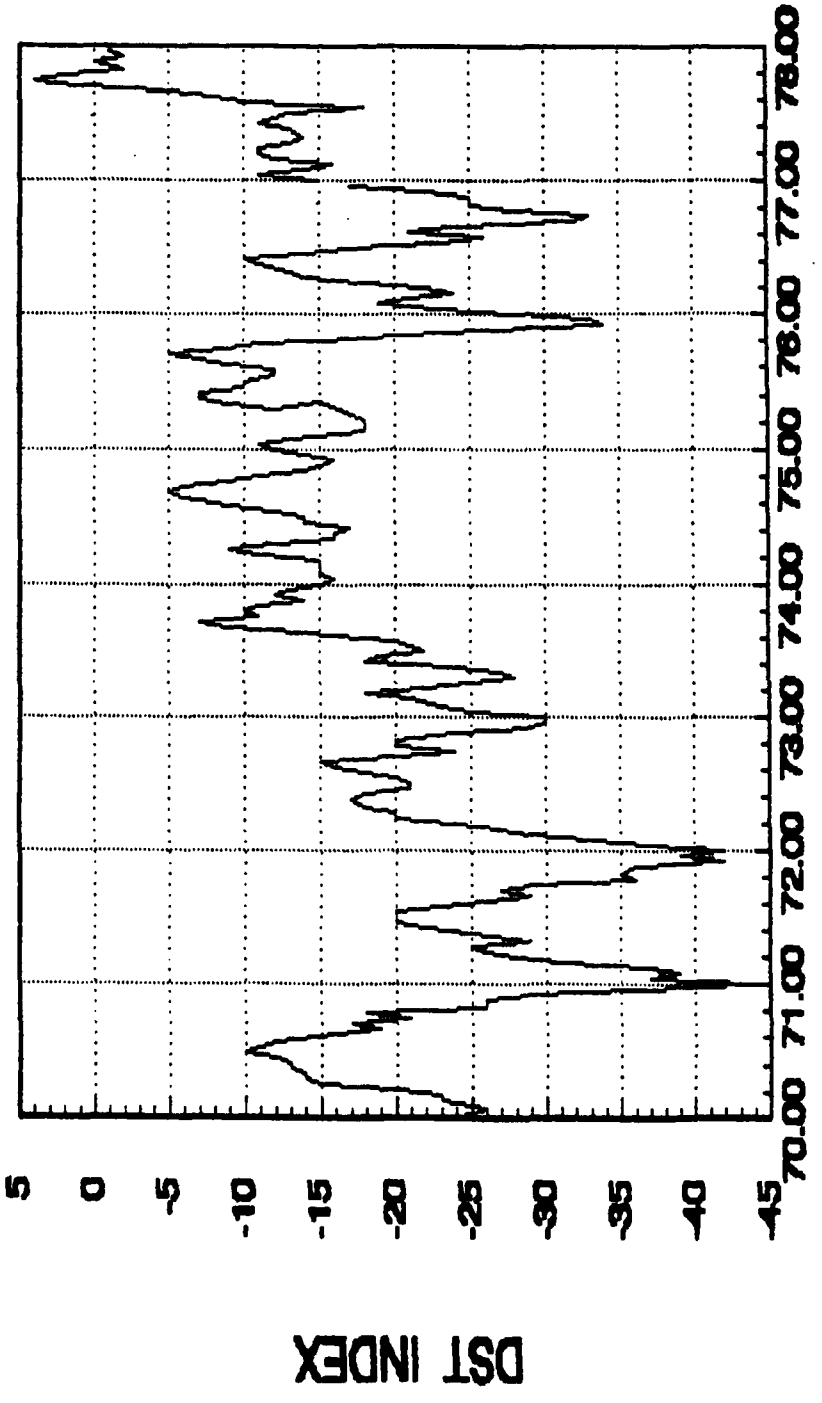

Figure 9
DST Index March 1977

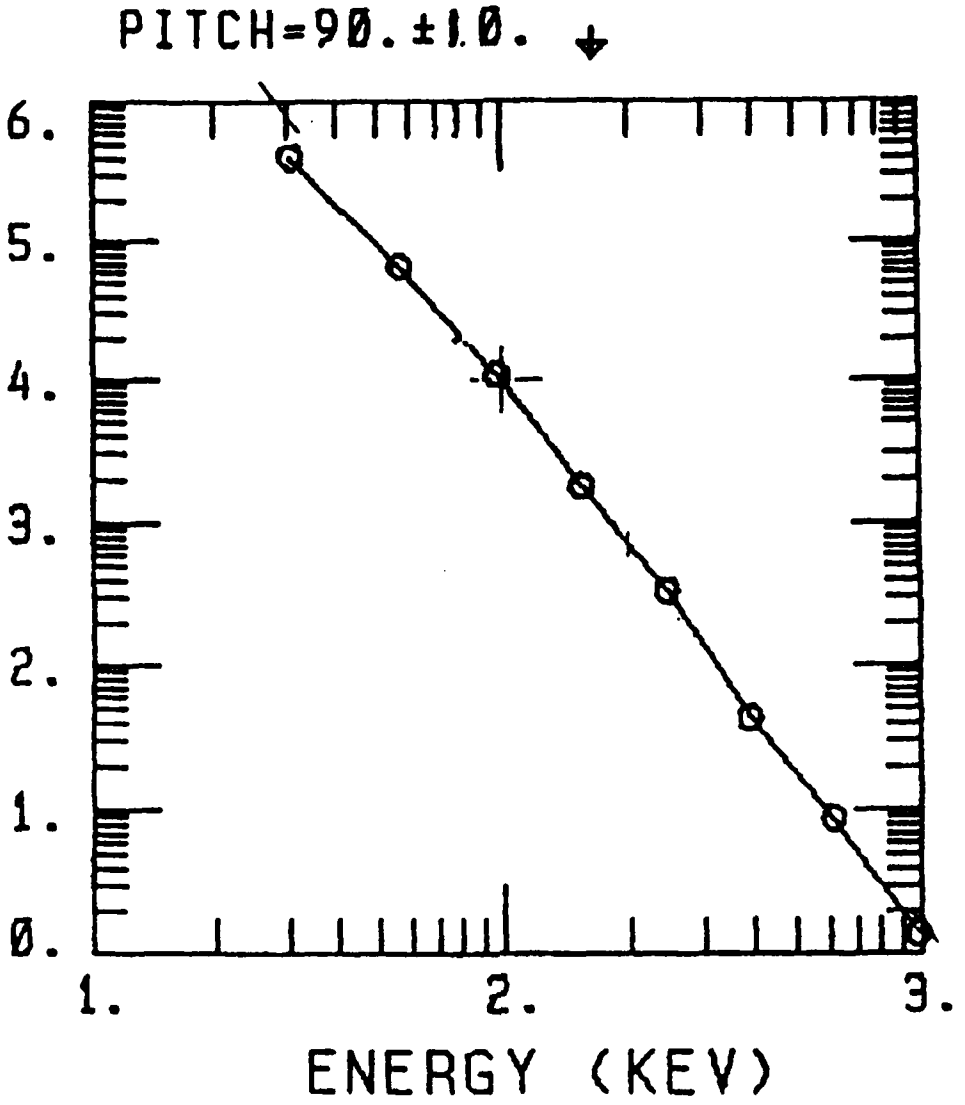

Figure 10
ISEE1 Data

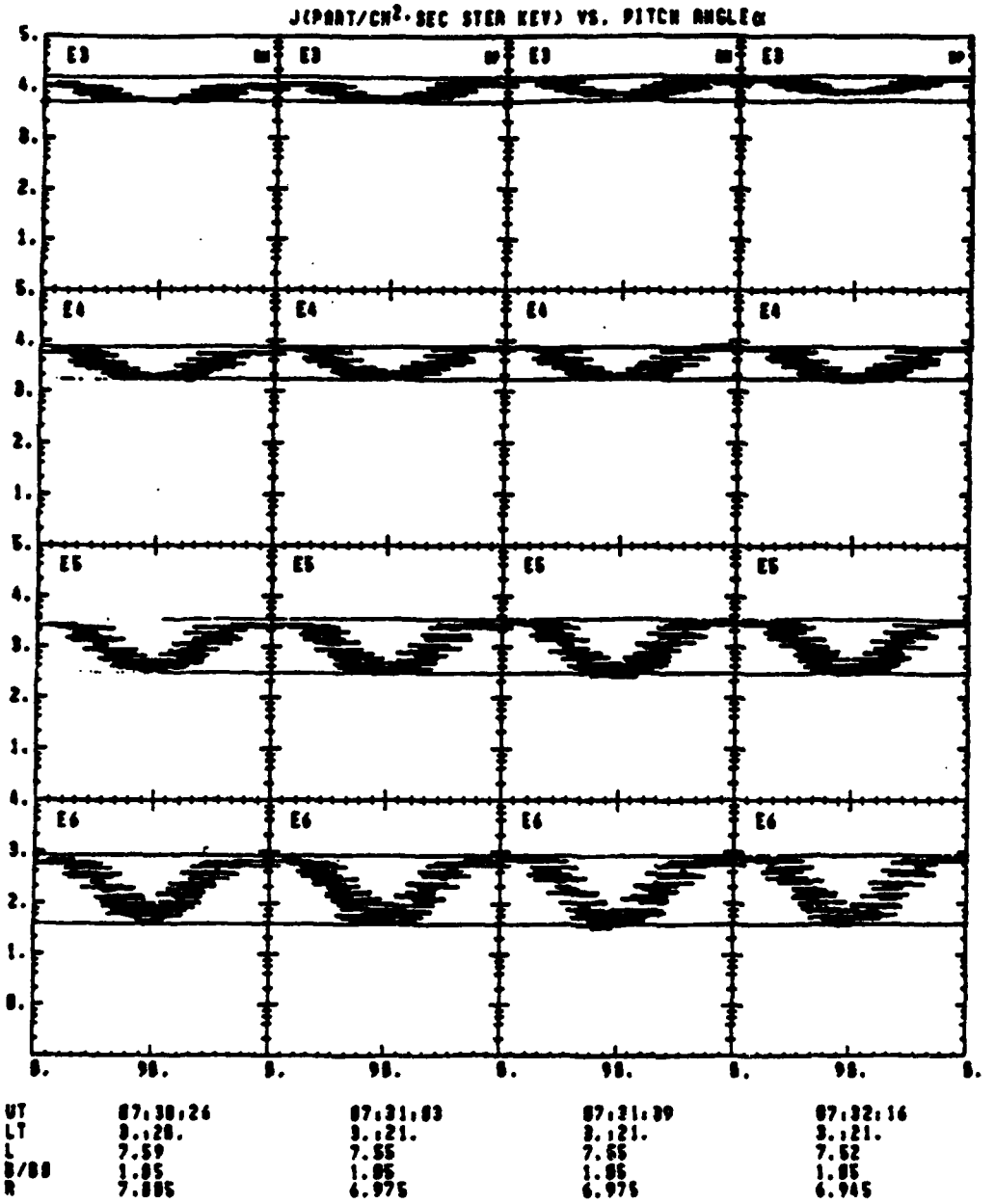

Figure 11
Electron Flux Dependence on Pitch Angle

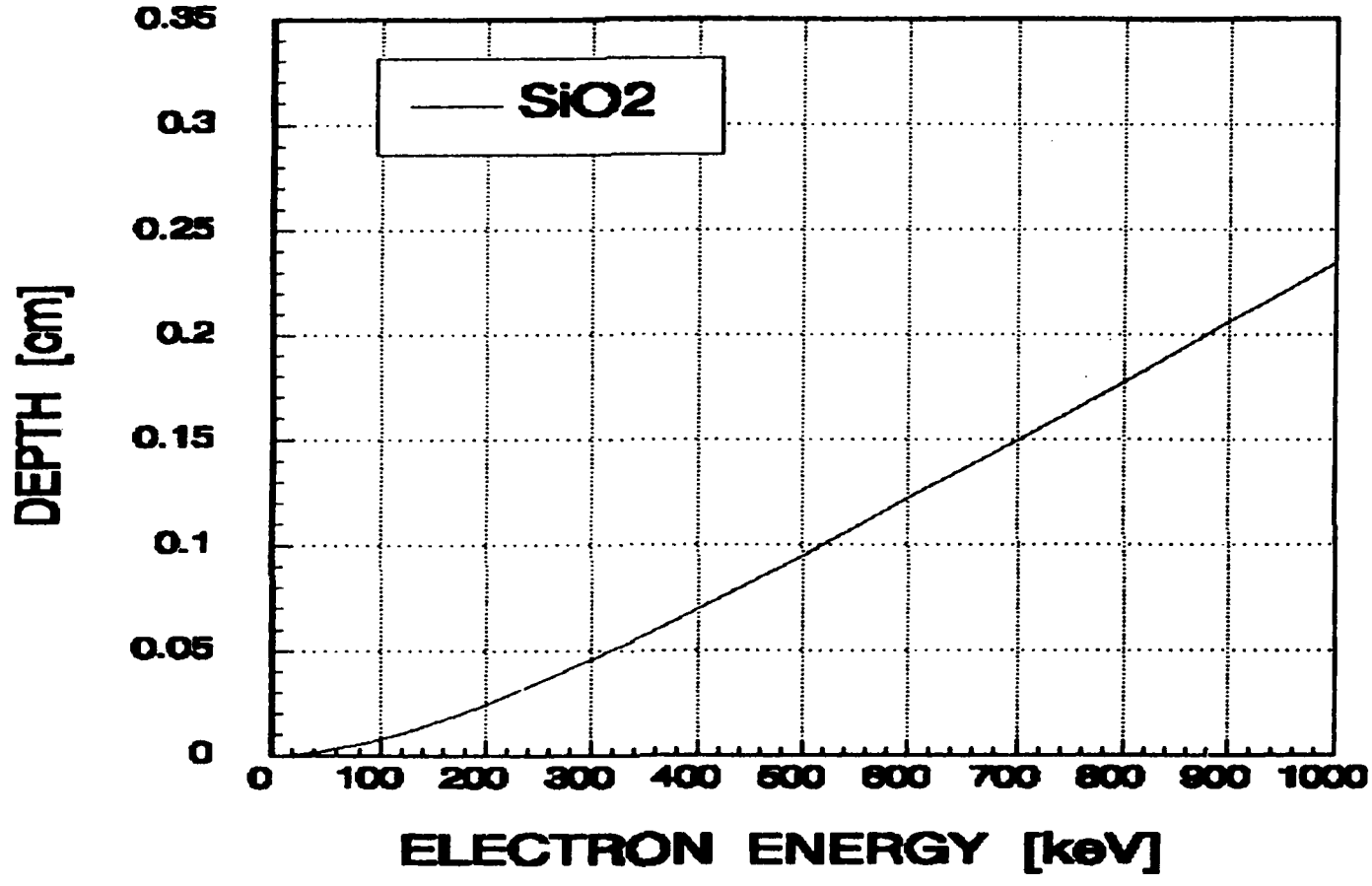

Figure 12
Electron Penetration Depth
Versus Energy in SiO_2
[Ref. 37:p. 123]

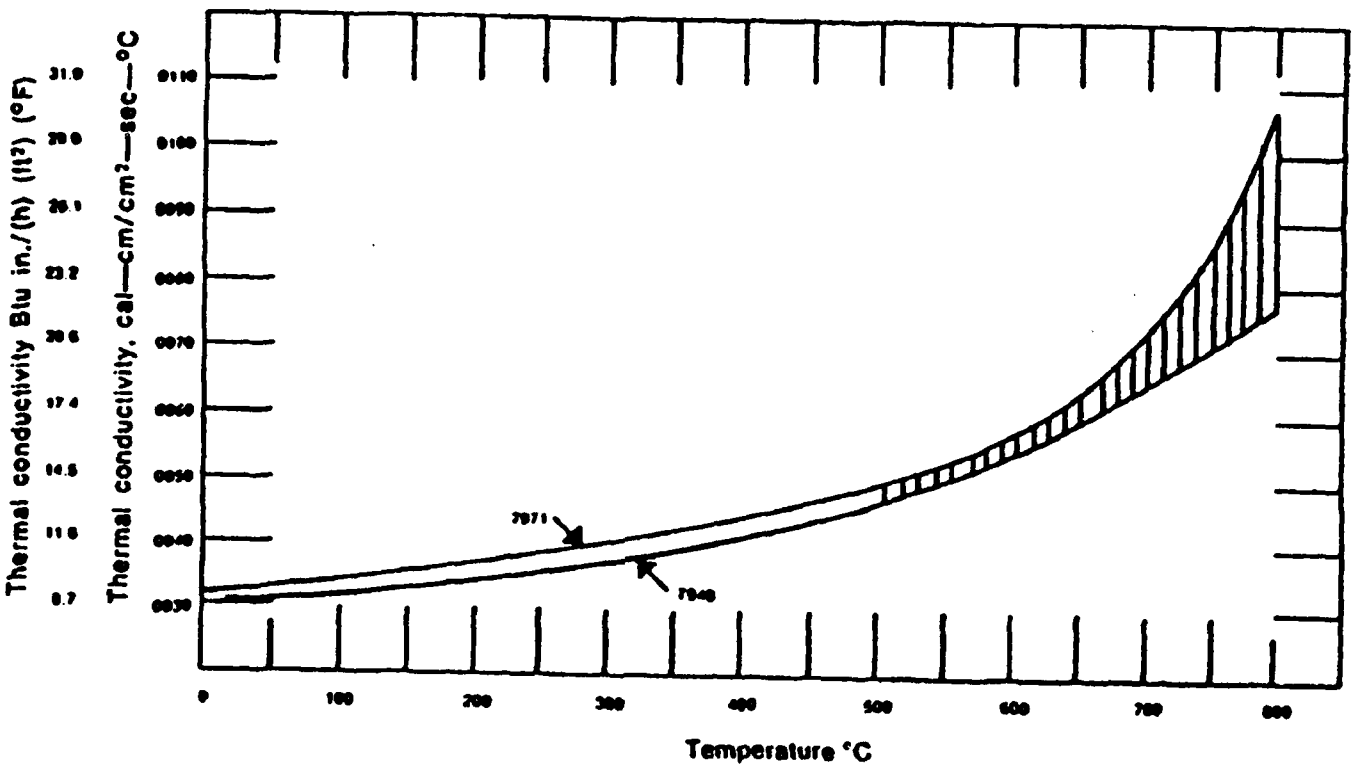

Figure 13
Conductivity of SiO_2 as a
Function of Temperature
[Ref. 44:p. 17]

DATE	DAY	CURRENT DENSITY (pA/cm^2)						
		>1 keV	>3 keV	>10 keV	>30 keV	>100 keV	>300 keV	>1000 keV
22 MAR 1979	81	13	11	5.9	1.3	0.18	0.03	-
28 MAR 1979	87	170	140	82	26	0.47	0.26	-
25 APR 1979	115	112	97	50	10	3.7	1.7	0.32
29 AUG 1979	241a	800	750	450	105	3.5	0.05	-
	241b	620	570	285	78	6.6	0.40	-
14 JUN 1980	166	160	130	75	13	3.7	1.8	0.46
22 APR 1981	112	300	270	165	56	3.7	0.33	0.02
23 APR 1981	113	245	220	142	46	2.5	0.38	0.025

Figure 14
Energetic Flux Levels
[Ref. 17:p. 360]

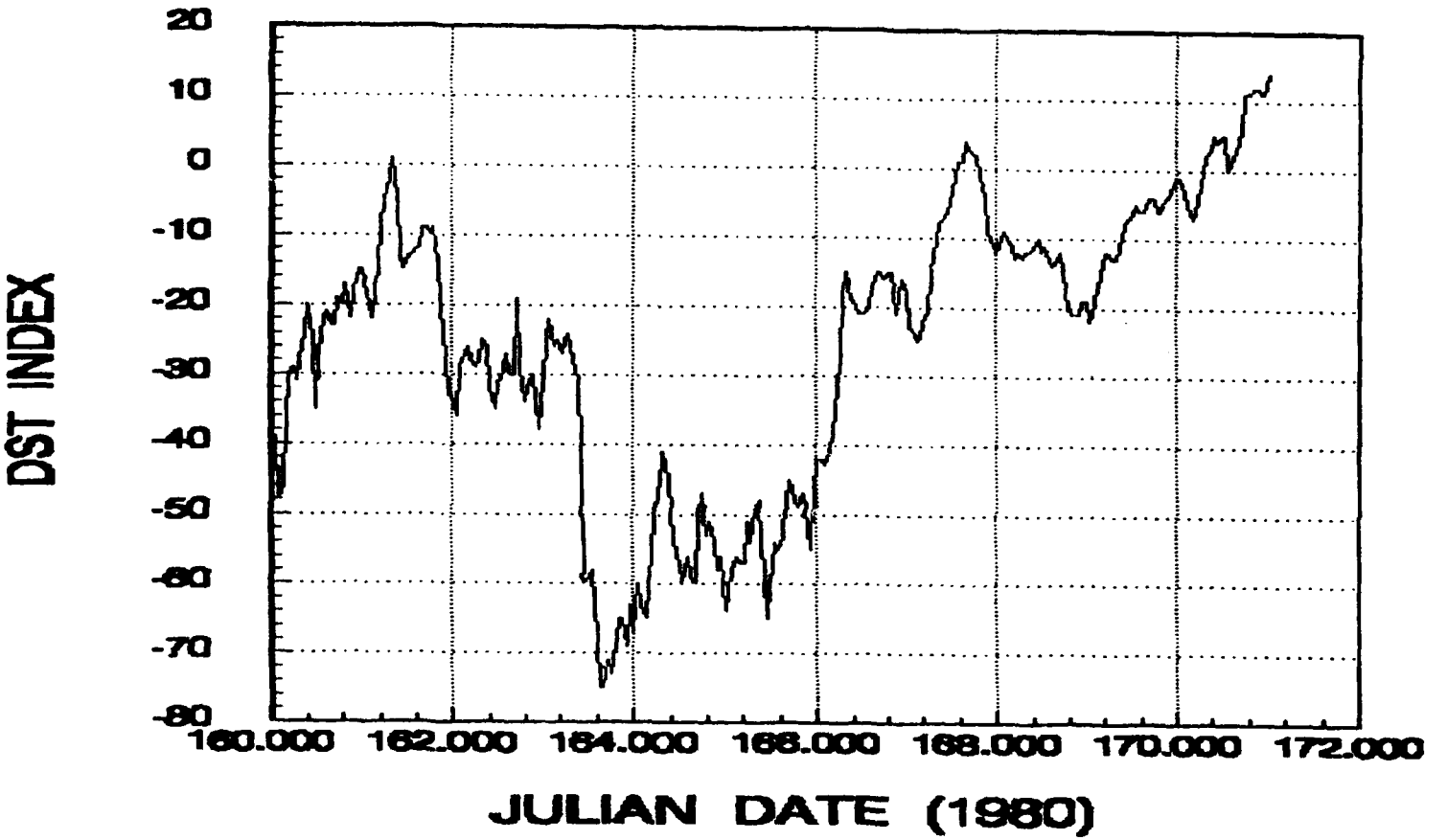

Figure 15
DST Index June 1980

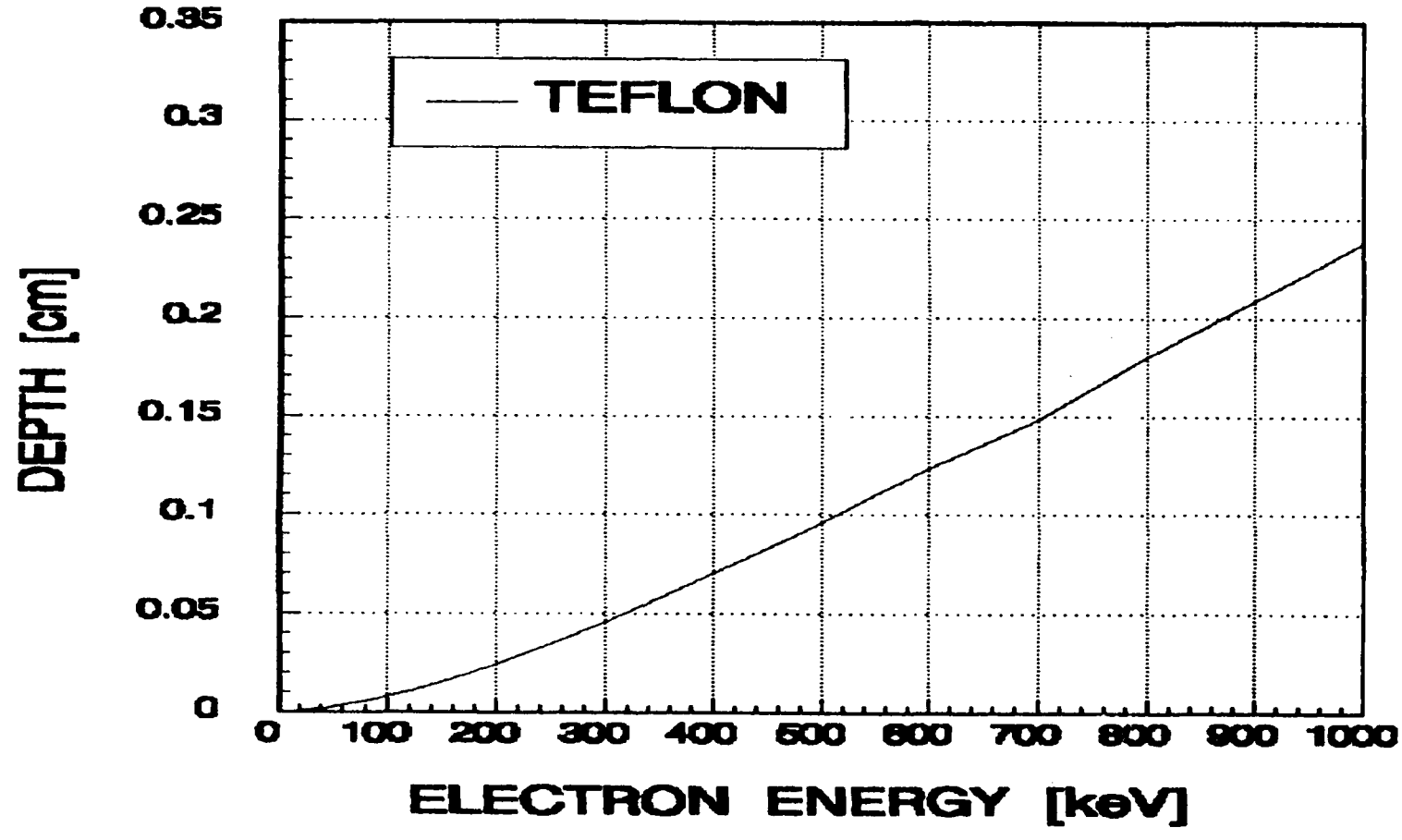

Figure 16
Electron Penetration Depth
Versus Energy in Teflon
[Ref. 37:p. 142]

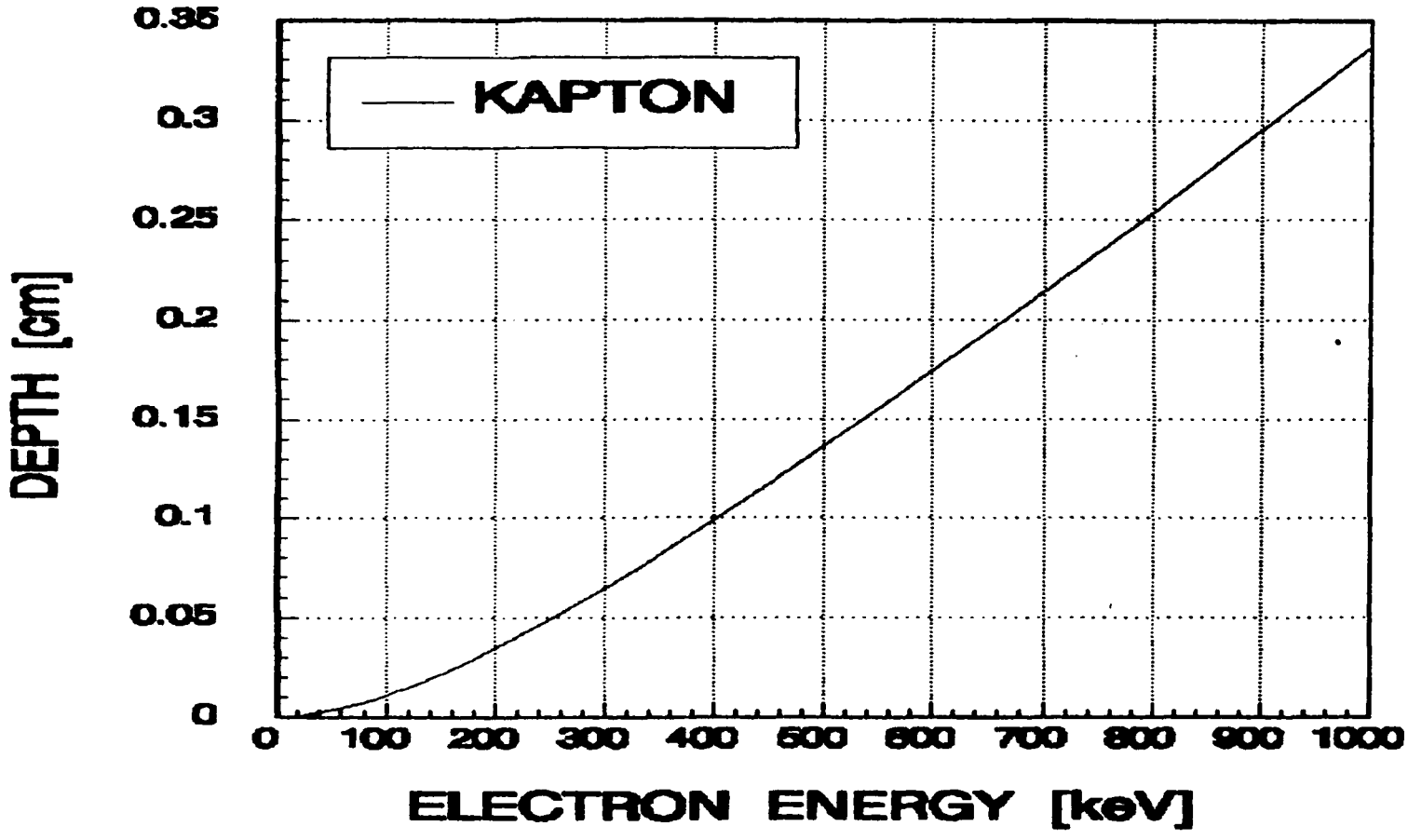

Figure 17
Electron Penetration Depth
Versus Energy in Kapton
[Ref. 37:p. 124]

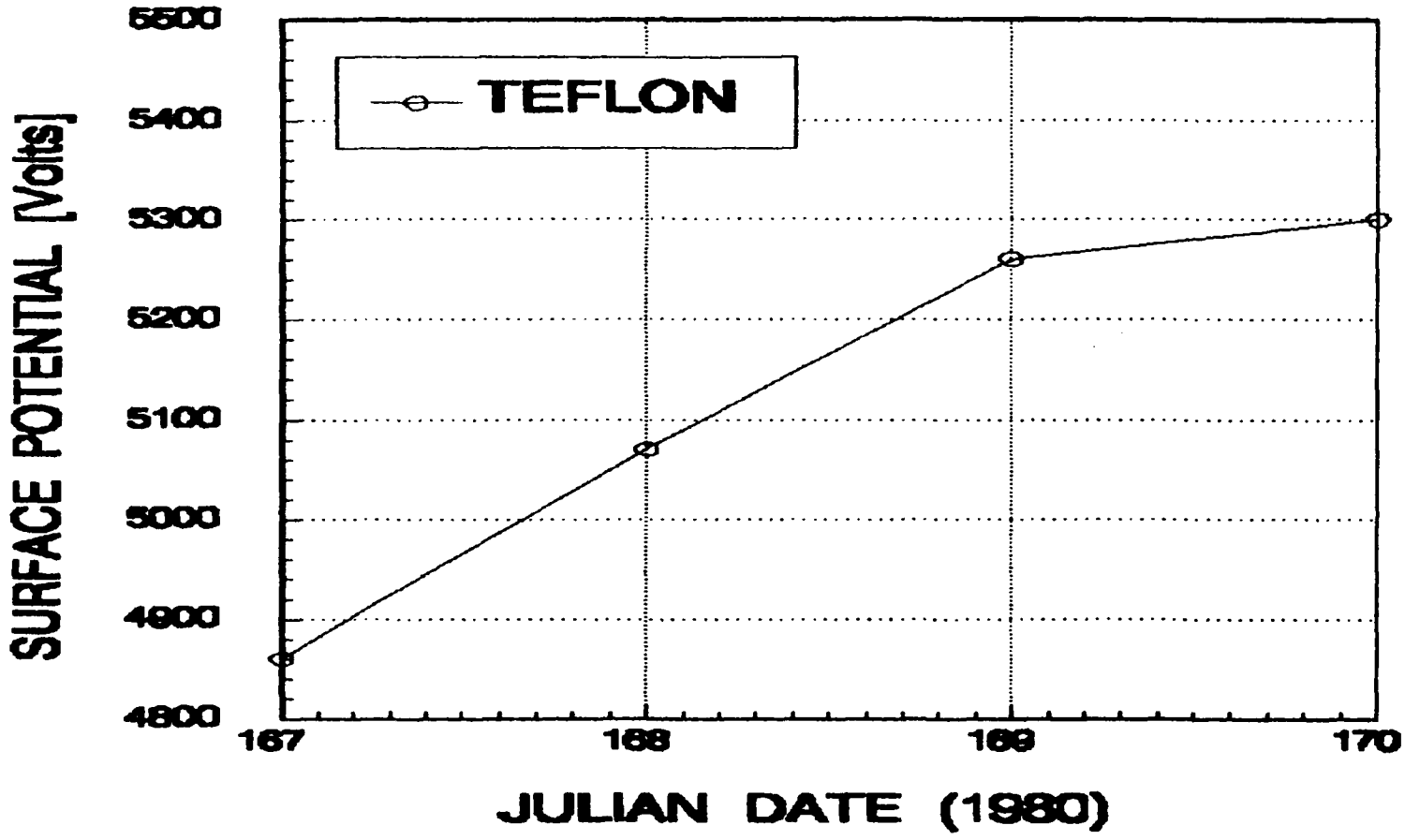

Figure 18
Teflon Surface Potential
(From SSPM) June 1980

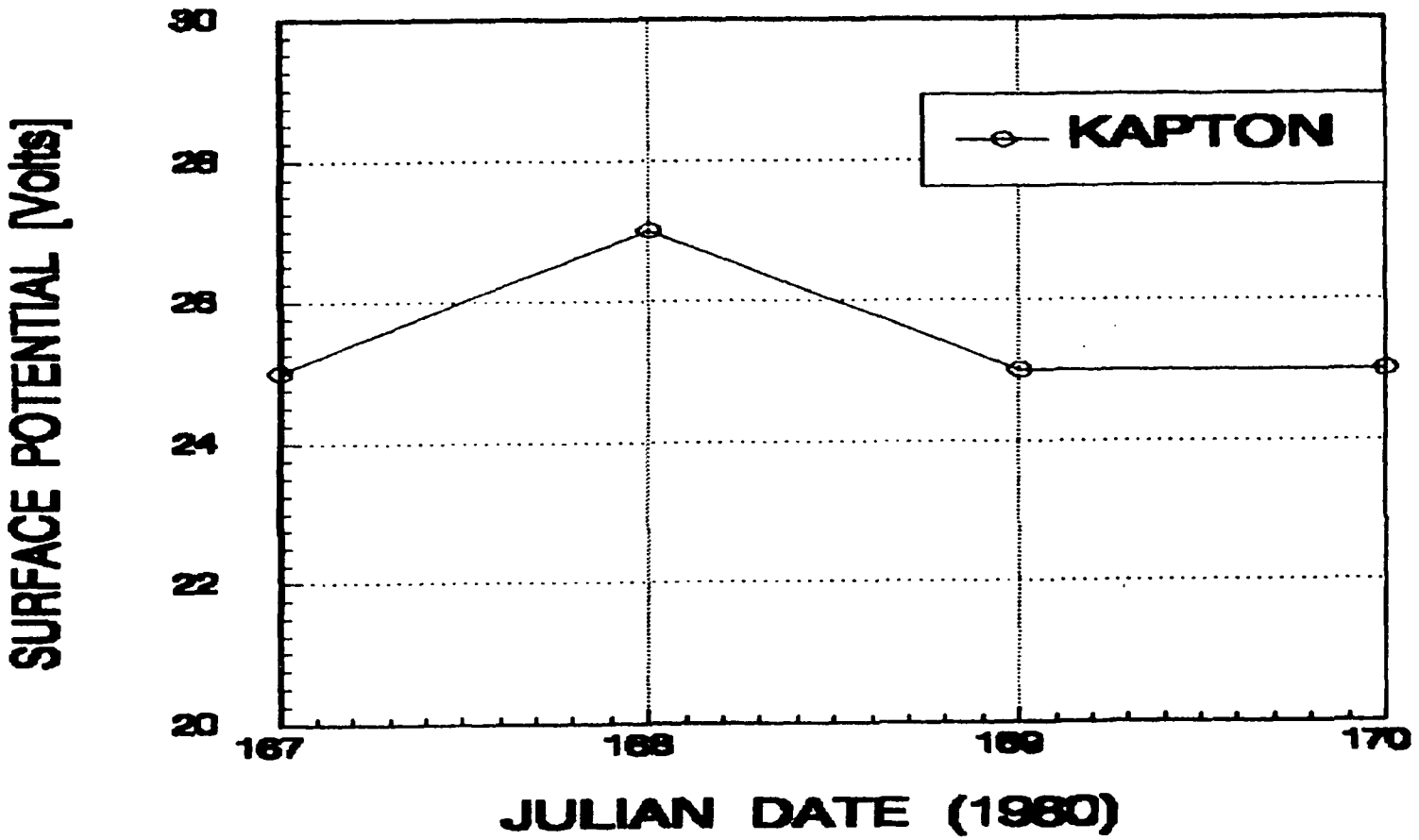

Figure 19
Kapton Surface Potential
(From SSPM) June 1980

TABLE 7. Correlation Coefficients of ϕ_f Versus Electron Flux

SC5 Energy Bin, keV	Day 114	Day 241	Day 363
0.62	−0.87	−0.10	−0.48
1.57	−0.72	+0.08	−0.28
4.4	−0.28	+0.25	+0.21
9.2	−0.36	+0.50	+0.58
23.8	+0.42	+0.83	+0.75
53.8	+0.94	+0.87	+0.87
96	+0.85	+0.01	+0.63
218	+0.92	−0.46	+0.38
335	+0.92	−0.28	+0.58
Number of Points	37	114	41

Figure 20
Correlation of Electron Energy to
Spacecraft Mainframe Potential
[Ref. 48:p. 1485]

APPENDIX C

```
C     ********************************************************
C     * THIS PROGRAM CALCULATES THE PRIMARY SURFACE CHARGING *
C     *      CURRENTS INVOLVED IN SPACECRAFT CHARGING        *
C     ********************************************************
C
C               ****VARIABLE DEFINITION****
C
C     JOT    = TOTAL CURRENT TO THE SURFACE
C     JPHOTO = PHOTOELECTRIC CURRENT
C     JSEC   = SECONDARY ELECTRON CURRENT
C     JBS    = BACKSCATTERED ELECTRON CURRENT
C     YM     = MAX SECONDARY YIELD FOR SURFACE MATERIAL
C     EM     = ENERGY WHERE YM OCCURS
C     Z      = EFFECTIVE ATOMIC NUMBER OF SURFACE MATERIAL
C
C     * THE PROGRAM CALULATES THE CURRENTS FOR AN ENVIRONMENT*
C     *      DESCRIBED BY TWO MAXWELLIAN DISTRIBUTIONS       *
C     KTi = THE ith PLASMA TEMPERATURE [keV]
C     Ni  = THE ith DENSITY [M**3]
C     TPi = THE ith PROTON TEMPERATURE
C
C     ****VARIABLE INITIALIZATION*****
      REAL JPHOTO,JSEC,JBS,JAMB
      REAL KT1,N1,Tp1,KT2,TP2,N2
      REAL YM,EM,Z
C
C      ***DATA FILES--INPUT***
C
C      *THE PROGRAM READS DATA FROM AN INPUT FILE, IPDATA.DAT*
C      *THE VARIALBES READ FROM THE FILE ARE GIVEN BELOW, AND*
C      * THE FORMAT STATEMENTS TELL HOW TO CONSTRUCT THE FILE*
C
C      **THE PROGRAM ALSO REQUIRES TWO FILES CONTAINING THE**
C      ** LAGUERRE ZEROS AND WEIGHTS FOR INTEGRATION THESE **
C      **THESE ARE CONTAINED IN THE FILES XI.DAT & WTS.DAT **
C
      OPEN (UNIT=1,FILE='WTS.DAT',STATUS='OLD')
      OPEN (UNIT=2,FILE='XI.DAT',STATUS='OLD')
      OPEN (UNIT=8,FILE='IPDATA.DAT',STATUS='OLD')
```

```
C     ****PROGRAM INPUTS****
C
C     ****READ FROM THE FILE****
      READ(8,110) KT1,Tp1,N1
      READ(8,110) KT2,Tp2,N2
      READ(8,120) YM,EM
      READ(8,130) Z
      REWIND 8
C
C     ***CONVERSION TO MKS FOR CALCULATIONS****
C
      KT1 = KT1*1.6E-16
      Tp1 = Tp1*1.6E-16
      KT2 = KT2*1.6E-16
      Tp2 = Tp2*1.6E-16
C
C     ****MAIN PROGRAM SECTION****
C
C     **SUBROUTINE CALLS**
C
      CALL PHOTOJ(JPHOTO)
      CALL AMBIENT(KT1,N1,KT2,N2,Tp1,TP2,JAMB)
      CALL SECOND(KT1,N1,KT2,N2,JSEC,YM,EM)
      CALL BACKES(KT1,N1,KT2,N2,JBS,Z)
C
C     ***FORMAT STATEMENTS***
C
  110 FORMAT (2F3.1,E8.2)
  120 FORMAT (F3.1,F5.1)
  130 FORMAT (F4.1)
  140 FORMAT (F7.1,1X,E10.4)
C
      END
C
C
C     *****SUBROUTINES*****
C
C     ****THIS MODULE CALCULATES THE PHOTOELECTRIC CURRENT****
C
      SUBROUTINE PHOTOJ(JPHOTO)
      REAL JPHOTO
      JPHOTO = (2.1E-5)/(1.602E-19)
      PRINT*,'JPHOTO = ',JPHOTO
      RETURN
      END
C
C     ***THIS MODULE CALCULATES THE AMBIENT PLASMA CURRENTS***
```

```
C
      SUBROUTINE AMBIENT(KT1,N1,KT2,N2,Tp1,Tp2,JAMB)
      REAL JAMB,N1,N2,Me,Mp,KT1,KT2,Tp1,Tp2,PI/3.141592/
      REAL JIONS1,JIONS2,JE1,JE2,JAMB1,JAMB2
C
C     ***VARIABLE DECLARATION & INITIALIZATION***
C
      Mp = 1.67E-27
      Me = 9.11E-31
C
      JE1 = N1*SQRT(KT1)/SQRT(PI*2.0*Me)
      JIONS1 = N1*SQRT(Tp1)/SQRT(PI*2.0*Mp)
      JAMB1 = JE1-JIONS1
      JE2 = N2*SQRT(KT2)/SQRT(PI*2.0*Me)
      JIONS2 = N2*SQRT(Tp2)/SQRT(PI*2.0*Mp)
      JAMB2 = JE2-JIONS2
      JAMB = JAMB1+JAMB2
      PRINT*,'JAMB = ',JAMB
      RETURN
      END
C
C     **SUBROUTINE TO CALCULATE THE SECONDARY ELECTRON EMISSION
C
      SUBROUTINE SECOND(KT1,N1,KT2,N2,JSEC,YM,EM)
      REAL M/9.11E-31/,PI/3.141592/,YM,EM
      REAL Wi,Xi,FX1,FX2,SUM1,SUM2,R1,R2,N1,N2
      REAL KT1,KT2,JSEC,JSEC1,JSEC2
      REAL FACT1,FACT2,RES1,RES2
      INTEGER J
C
C     ***VARIABLE DEFINITION***
C
      EM = EM*1.6E-16
C
C     ***LAGUERRE INTEGRATION***
C
      SUM1 = 0.0
      SUM2 = 0.0
      DO 10 J=1,5
        READ (1,*)Wi
        READ (2,*)Xi
        R1 = (-2.0)*SQRT((KT1/EM)*Xi)
        FX1 = (Xi**2.0)*EXP(R1)
        RES1 = Wi*FX1
        SUM1 = SUM1 + RES1
        R2 = (-2.0)*SQRT((KT2/EM)*Xi)
        FX2 = (Xi**2.0)*EXP(R2)
```

```
      RES2 = Wi*FX2
      SUM2 = SUM2 + RES2
   10 CONTINUE
      FACT1 = (7.4*N1/SQRT(2*PI*M))*(YM/EM)*(KT1**1.5)
      JSEC1 = FACT1*SUM1
      FACT2 = (7.4*N2/SQRT(2*PI*M))*(YM/EM)*(KT2**1.5)
      JSEC2 = FACT2*SUM2
      JSEC = JSEC1+JSEC2
      REWIND 1
      REWIND 2
      PRINT*,'JSECS= ',JSEC
      RETURN
      END
C
C     ****THIS MODULES CALCULATES THE BACKSCATTERED ELECTRONS
C
      SUBROUTINE BACKES(KT1,N1,KT2,N2,JBS,Z)
C     *****NUMERICAL INTEGRATION OF BACKSCATTERED ELECTRONS*****
C
C     ****VARIABLE DEFINITION*****
      REAL JBS,JBS1,JBS2,R1,R2,KTEV1,KTEV2
      REAL KT1,KT2,B,N1,N2,Z,PI/3.141592/
      REAL M/9.11E-31/,C1,C2,C11,C12,C21,C22
      REAL RES1,RES2,FX1,FX2,SUM1,SUM2
C
C     ****CALCULATIONS****
C
      KTEV1 = KT1/1.6E-16
      KTEV2 = KT2/1.6E-16
      B = 10.0*(1-(2/2.7183))*(0.037*Z)
      DO 20 I =1,5
      READ (1,*) Wi
      READ (2,*) Xi
      R1 = -Xi*KTEV1/5.0
      FX1 = (1.0-(0.05/(Xi*KTEV1)))*(B+EXP(R1))*Xi
      RES1 = Wi*FX1
      SUM1 = SUM1 +RES1
      R2 = -Xi*KTEV2/5.0
      FX2 = (1.0-(0.05/(Xi*KTEV2)))*(B+EXP(R2))*Xi
      RES2 = Wi*FX2
      SUM2 = SUM2 +RES2
   20 CONTINUE
      C11 = 0.1*N1/SQRT(PI*M*2.0)
      C12 = SQRT(KT1)
      C1  = C11*C12
      JBS1 = SUM1*C1
      C21 = 0.1*N2/SQRT(PI*M*2.0)
```

```
C22 = SQRT(KT2)
C2  = C21*C22
JBS2 = SUM2*C2
JBS = JBS1+JBS2
REWIND 1
REWIND 2
PRINT*,'JBS = ',JBS
RETURN
END
```

LIST OF REFERENCES

1. DeForest, S. E., "Spacecraft Charging at Synchronous Orbit," *Journal of Geophysical Research*, v. 77, February 1977.

2. Fredricks, R. W. and Scarf, F. L., "Observations of Spacecraft Charging Effects in Energetic Plasma Regions," *Photon and Particle interactions with Surfaces in Space*, ed. R. J. L. Grard, D. Reidel Publishing Company, 1972.

3. Pike C. P., and Bunn, M. H., "A Correlation Study Relating Spacecraft Anomalies to Environmental Data," *Spacecraft Charging by Magnetospheric Plasmas, Vol. 47, AIAA*, ed. A. Rosen, AIAA with MIT Press, 1976.

4. McPherson, D. A. and Schober W. R., "Spacecraft Charging at High Altitudes: The SCATHA Satellite Progam," idem Ref. 3.

5. Koons, H. C., "Summary of Environmentally Induced Electrical Discharges on the P78-2 (SCATHA) Satellite," *Journal of Spacecraft and Rockets*, v. 20, n. 5, September-October 1983.

6. Garrett, H. B., "Spacecraft Charging: A Review," *Space Systems and Their Interactions with the Earth's Space Environment, Vol. 71, AIAA*, ed. H. B. Garrett and C. P. Pike, AIAA with New York University, 1980.

7. Shaw, R. R., Nanevica, J. E., and Adamo, R. C., "Observations of Electrical Discharge Caused by Differentail Satellite Charging," idem Ref. 3.

8. Meulenberg, A. Jr., "Evidence for a New Discharge Mechanism for Dielectics in a PLasma," idem Ref. 3.

9. Vampola, A. L., "Thick Dielectric Charging on High-Altitude Spacecraft," *Journal of Electrostatics*, v. 20, 1987.

10. Wrenn, G.L., and Johnstone, A. D., "Spacecraft Charging: Meteosat Experience," *The Aerospace Environment at High Altitudes and Its Implications for Spacecraft Charging and Communications*, AGARD Conference Proceedings No. 406, The Hague Netherlands, 1986.

11. Wadham P. N., "The Effects of Electrostatic Discharges Phenomena on Telesat's Domestic Communications Satellite," idem Ref. 10.

12. Barnett, A. and McNutt, R. L. Jr., "Charging Effects Observed on Voyager 1 Near Jupiter," *Spacecraft/PlasmaInteractions and their Influence on Field and Particle Measurements*, Proceedings of the 17th ESLAB Symposium Noordwijk, The Netherlands, ESA SP-198, November 1983.

13. Wenaas, E. P., "Spacecraft Charging Effects by the High- Energy Environment," *IEEE Transactions on Nuclear Science*, v. NS-24, n. 6, December 1977.

14. Fredrickson, A. R., "Electric Discharge Pulses in Irradiated Solid Dielectrics in Space," *IEEE Transactions on Electrical Insulation*, v. EI-18, n. 3, June 1983.

15. Fredrickson, A. R., "Radiation Induced Dielectric Charging," idem Ref. 5.

16. Fredrickson, A. R, and others, *Spacecraft Dielectrics Material Properites and Spacecraft Charging, Vol 107 AIAA*, AIAA, 1986.

17. Reagan, J. B., et al., "Space Charging Currents and Their Effects on Spacecraft Systems," *IEEE Transactions on Electrical Insulation*, v. EI-18, n.3, June 1983.

18. Beers, B. L., et al., "Electron Transport Model of Dielectric Charging," *Spacecraft Charging Technology 1978*, NASA Conference Publication 2071, AFGL-TR-79-0082.

19. Tabata, T., and Ito, R., "An Algorithm for the Energy Deposition by Fast Electrons," *Nuclear Science and Engineering*, v. 53, 1974.

20. Telephone conversation between N. J. Stevens, M2/2165, TRW, and the author, January 1990.

21. Telephone conversation between A. R. Fredrickson, PHP, AFG, and the author, February 1990.

22. Vampola, A. L., "Radiation Effects on Space Systems and Their Modeling." idem Ref. 5

23. Freeman, J. W., and Maguire, J.J., "Gross Local-Time Particle Asymmetries at the Synchronous Orbit Altitude," *Journal of Geophysical Research*, v. 72, n. 21, Nov 1967.

24. DeForest, S. E., and McIlwain, C. E., "Plasma Clouds in the Magnetosphere," *Journal Geophysical Research*, v. 76, n.16, June 1971.

25. Mandell, M. J., et al., "The Decrease in Effective Photocurrents Due to Saddle Points in Electrostatic Potentials Near Differentially Charged Spacecraft," *IEEE Transactions on Nuclear Science*, v. NS-25, 1978.

26. Olsen, R. C., Whipple, E.C., and McIlwain, C.E., "Observations of Differential Charging Effects on ATS 6," *Journal of Geophysical Research*, v. 86, n. A8, August 1981.

27. Olsen, R. C., and Whipple, E. C., "An Unusual Charging Event on ISEE1," *Journal of Geophysical Reasearch*, v. 93, n. A6 June 1988.

28. Adamo, R. C., and Matarrese, J. R., "Transient Pulse Monitor Data from the P78-2 (SCATHA) Spacecraft," *Journal of Spacecraft and Rockets*, September-October 1983.

29. Interview between R. C. Olsen, Naval Postgrduate School, Monterey, CA, and the author, March 1990.

30. Olsen, R. C., "A Threshold Effect for Spacecraft Charging," *Journal of Geophysical Research*, v. 88, n. A1, January 1983.

31. Grard, R. J. L., Knott, K., and Pedersen, A., "The Influence of Photoelectron and Secondary Electron Emission of Electric Field Measurements in the Magnetosphere and Solar Wind," *Photon and Particle Interactions with Surfaces in Space*, ed. R. J. L. Grard, D. Reidel Publishing Company, 1972.

32. Garrett, H. B., "The Geosynchronous Plasma Environment," paper presented at the American Institue of Aeronautics and Astronautics Aerospace Sciences Meeting, 28th, Reno, Nevada, January 8-11 1990.

33. Whipple, E. C., "Potentials of Surfaces in Space," *Reports on Progress in Physics*, v. 44, 1981.

34. Knott, K., "The Equilibrium Potential of a Magnetospheric Satellite in an Eclipse Situation," *Planetary and Space Science*, v. 20, 1972.

35. Olsen, R. C., *Differential and Active Charging Results from the ATS Spacecraft*, Ph.D. Dissertation, University of California, San Diego, California, 1980.

36. Rudie, N. J., *Principles and Techniques of Radiation Hardening*, Vol. I, Western Periodical Company, 1980.

37. U. S. Department of Commerce, National Bureau of Standards Report NBSIR 82-2550-A, *Stopping Power and Ranges of Electrons and Positrons*, by M. J. Berger and S. M. Seltzer, December 1982.

38. Fredrickson, A. R., "Radiation Induced Currents and Conductivity in Dielectrics," *IEEE Transactions on Nuclear Science*, v. NS-24, n. 6, December 1977.

39. Wall, J. A., et al., "Results of Literatur Search on Dielectric Properites and Electron Ineraction Phenomena Related to Spacecraft Charging," *Proceedings of the Spacecraft Charging Technology Conference*, ed. C.P. Pike and R. R. Lovell, AFGL-TR-77-0051, February 1977.

40. Mizera, P. F., et al., "First Results of Material Charging in the Space Environment," *Applied Physics Letters*, v. 37, August 1980.

41. Davidson, G. T., et al., "Observations of Intense Trapped Electon Fluxes at Synchronous Altitudes," *Journal of Geophysical Research*, v. 93, n. A1, January 1988.

42. Russell, C.T., and Southwood, D. J., editors, *The IMS Source Book*, American Geophysical Union, 1982.

43. Optical Coating Laboratory, Inc., Specification: Solar Cell Covers with Conductive Coating and Contacts.

44. Corning Glass Works, *Properties of Corning's Glass and Glass Ceramic Families*, December 1979.

45. Baker, D. N., et al., "Deep Dielectric Charging Effects Due to High Energy Electrons in Earth's Outer Magnetosphere," *Journal of Electrostatics*, v.

46. Reagan, J. B., et al., "Role of Energetic Partilce in Charging/Discharging of Spacecraft Dielectrics," *Spacecraft Charging Technology 1980*, NASA Conference Publication 2182, AFGL- TR-81-0270, 1980.

47. Interview between R. C. Olsen, Naval Postgraduate School, Monterey, California, and the author, December 1989.

48. Mullen, E. G., et al., "SCATHA Survey of High Level Spacecraft Charging in Sunlight," *Journal of Geophysical Research*, February 1986.

49. Tascione, T. F., *Introduction to the Space Environment*, Orbit Book Company, 1988.

50. Caprara, G., *The Complete Encyclopedia of Space Satellites*, Portland House, 1986.

INITIAL DISTRIBUTION LIST

1.	Defense Technical Information Center Cameron Station Alexandria, VA 22304-6145	2
2.	Library, Code 0142 Naval Postgraduate School Monterey, CA 93943-5002	2
3.	Department Chairman, Code 61 Department of Physics Naval Postgraduate School Monterey, CA 93943-5000	2
4.	Dr. R. C. Olsen, Code 61OS Department of Physics Naval Postgraduate School Monterey, CA 93943-5000	20
5.	Dr. X. K. Maruyama, Code 61MX Department of Physics Naval Postgraduate School Monterey, CA 93943-5000	1
6.	Dr. D. J. Williams Johns Hopkins University, APL Johns Hopkins Road Laurel, MD 20707-6099	1
7.	Dr. P. Mizera M5/620 Aerospace Corporation P.O. Box 92957 Los Angeles, CA 90009	1
8.	Dr. J. L. Roeder M2/260 Aerospace Corporation P.O. Box 92957 Los Angeles, CA 90009	1

9. Dr. H. Koons — 1
M2/260
Aerospace Corporation
P.O. Box 92957
Los Angeles, CA 90009

10. Dr. J. Fennell — 1
M2/259
Aerospace Corporation
P.O. Box 92957
Los Angeles, CA 90009

11. Dr. D. Croley — 1
M2/259
Aerospace Corporation
P.O. Box 92957
Los Angeles, CA 90009

12. Dr. J. B. Reagan — 1
Lockheed Palo Alto Research Laboratories
3251 Hanover St.
Palo Alto, CA 94304

13. Dr. R. Nightingale — 1
Lockheed Palo Alto Research Laboratories
3251 Hanover St.
Palo Alto, CA 94304

14. Dr. J. Quinn — 1
Lockheed Palo Alto Research Laboratories
3251 Hanover St.
Palo Alto, CA 94304

15. Dr. D. Baker — 1
Code 690
NASA/GSFC
Greenbelt, MD 20771

16. Dr. E. C. Whipple — 1
Center for Astrophysics and Space Science
University of California at San Diego
La Jolla, CA 92093

17. Dr. C. E. McIlwain 1
Center for Astrophysics and Space Science
University of California at San Diego
La Jolla, CA 92093

18. Dr. Forest Mozer 1
Space Sciences Laboratory
University of California
Berkeley, CA 94720

19. Dr. N. J. Stevens 1
M2/2165
TRW Space and Technology Group
One Space Park
Redondo Beach, CA 90278

20. Dr. A. R. Fredrickson 1
Air Force Geophysical Laboratory/PHP
Hanscom AFB, MA 01731

21. Dr. I. Katz 1
S-Cubed
P.O. Box 1620
La Jolla, CA 92038-1620

22. Dr. M. Mandell 1
S-Cubed
P.O. Box 1620
La Jolla, CA 92038-1620

23. Dr. V. Davis 1
S-Cubed
P.O. Box 1620
La Jolla, CA 92038-1620

24. Dr. R. D. Belian 1
Group SST-8
MS D438
Los Alamos National Laboratory
P. O. Box 1663
Los Alamos, NM 87545

25. Dr. G. Berzins — 1
Los Alamos National Laboratory
P. O. Box 1663
Los Alamos, NM 87545

26. Dr. T. Cayton — 1
SST-8
MS D438
Los Alamos National Laboratory
P. O. Box 1663
Los Alamos, NM 87545

27. Mr. Gracen Joiner — 1
Code 1114SP
Office of Naval Research
800 N. Quincy St.
Arlington, VA 22217

28. Commander — 1
Naval Space Command
Attn: Code N155
Dahlgren, VA 22448

29. United States Space Command — 1
Attn: Technical Library
Peterson AFB, CO 80914

30. Director — 1
Navy Space Systems Division (OP-943)
Washingtom, DC 20350-2000

31. Space Systems Academic Group, Code 72 — 1
Naval Postgraduate School
Monterey, CA 93943-5000

32. Space Systems Curricular Office, Code 39 — 1
Naval Postgraduate School
Monterey, CA 93943-5000

33. M. E. Young, LT, USN — 1
1472 Harwick Court
Crofton, MD 21114